# UC Irvine

## UC Irvine Electronic Theses and Dissertations

### Title

Developing Fluorescence Lifetime Libraries based on Silica Shells

### Permalink

https://escholarship.org/uc/item/91f52324

### Author

Deng, Tingwei

### Publication Date

2024

### Copyright Information

This work is made available under the terms of a Creative Commons Attribution License, available at https://creativecommons.org/licenses/by/4.0/

Peer reviewed|Thesis/dissertation

eScholarship.org Powered by the California Digital Library
University of California

UNIVERSITY OF CALIFORNIA,
IRVINE

# Developing Fluorescence Lifetime Libraries based on Silica Shells

DISSERTATION

submitted in partial satisfaction of the requirements
for the degree of

DOCTOR OF PHILOSOPHY

in Materials Science and Engineering

by

Tingwei Deng

Dissertation Committee:
Associate Professor Jered B. Haun, Chair
Associate Professor Michelle Digman
Professor Regina Ragan

2024

© 2024 Tingwei Deng

# DEDICATION

To

my family and friends

in recognition of their love and support

# TABLE OF CONTENTS

LIST OF FIGURES ..... vi

LIST OF TABLES ..... vii

LIST OF EQUATIONS ..... viii

ACKNOWLEDGMENTS ..... ix

VITA ..... x

ABSTRACT OF THE DISSERTATION ..... xii

CHAPTER 1 Introduction ..... 1

CHAPTER 2 Background ..... 5

2.1 Breast cancer overview ..... 5

2.2 Molecular multiplexing techniques ..... 6

2.2.1 Immunohistochemistry ..... 6

2.2.2 Immunofluorescence ..... 8

2.2.3 Mass Spectrometry ..... 10

2.2.4 Flow Cytometry ..... 12

2.2.5 Hyperspectral Imaging ..... 14

2.3 Fluorescence Lifetime Imaging Microscopy and Phasor Approach ..... 15

2.3.1 Fluorescence Lifetime and Quenching ..... 15

2.3.2 Fluorescence lifetime imaging microscopy ..... 16

2.3.3 Phasor approach to FLIM and Linear combination ..... 18

2.4 Nanoparticles ..... 21

2.4.1 Nanoparticle and its application ..... 21

2.4.2 Silica particle ..... 23

2.4.3 Biomedical applications of silica nanoparticles ..... 25

2.4.4 Quantum dots basic ..... 28

CHAPTER 3 Developing Nanoprobes with Silica Shells ..... 31

3.1 Introduction ..... 31

3.2 Materials and Methods ..... 32

3.2.1 Materials ..... 32

3.2.2 Preparation of Silica Particles via Reverse Microemulsion ..... 33

3.2.3 Primary PEGylation of Silica Particles....35
3.2.4 Backfilled PEGylation of Silica Particles....36
3.2.5 Antibody Modification....36
3.2.6 Immunoconjugation....37
3.2.7 Cell Culture and Cell labeling....38
3.2.8 Techniques....39
3.2.9 Calibration curve for CZ QDs concentration....42
3.3 Results and Discussion....43
3.3.1 Tetrazine effect in Primary PEGylation....43
3.3.2 Backfill PEGylation Optimization....45
3.3.3 Cell Staining to determine Specific Bindings....48
3.4 Conclusions....51
CHAPTER 4 Measuring Lifetime of Quantum dots with Silica Shells using FLIM....52
4.1 Introduction....52
4.2 Materials and Methods....54
4.2.1 Materials....54
4.2.2 Modification of Dark Quencher and silica particle preparation....55
4.2.3 Primary PEGylation of Silica Particles....55
4.2.4 Backfilled PEGylation of Silica Particles....56
4.2.5 Techniques....56
4.3 Results and Discussion....57
4.3.1 Size measurement of QD with Silica Shells....57
4.3.2 Emission measurement of QD with Silica Shells....59
4.3.3 Lifetime measurement of QD with Silica Shells....61
4.4 Conclusion....64
CHAPTER 5 Measuring Lifetime of Organic Dyes with Silica Shells using FLIM....65
5.1 Introduction....65
5.2 Materials and Methods....65
5.2.1 Materials....65
5.2.2 Modification of Organic dyes and Silica Particle Preparation....66
5.2.3 Primary PEGylation of Silica Particles....67
5.2.4 Backfilled PEGylation of Silica Particles....67
5.2.5 Techniques....68
5.3 Results and Discussion....68

5.3.1 Size measurement of Dye with Silica Shells ..... 68
5.3.2 Emission measurement of Dye with Silica Shells ..... 69
5.3.3 Lifetime measurement of Dye with Silica Shells ..... 72
5.4 Conclusion ..... 74
CHAPTER 6 Application of Silica Probes on Breast Cancer Cells using FLIM ..... 75
6.1 Introduction ..... 75
6.2 Materials and Methods ..... 76
6.2.1 Materials ..... 76
6.2.2 Modification of Organic dyes ..... 76
6.2.3 Primary PEGylation of Silica Particles ..... 77
6.2.4 Backfilled PEGylation of Silica Particles ..... 78
6.2.5 Antibody Modification ..... 78
6.2.6 Cell Culture and Cell labeling ..... 78
6.2.7 Techniques ..... 79
6.3 Results and Discussion ..... 80
6.3.1 Stability Test of Silica Shells ..... 80
6.3.2 Lifetime measurement of silica probes on cells ..... 81
6.3.3 Design of tumor panel ..... 85
6.4 Conclusion ..... 86
CHAPTER 7 Conclusions and Future Directions ..... 87
REFERENCES ..... 90

# LIST OF FIGURES

Figure 2.1 The standard workflow for chromogenic immunohistochemistry using the indirect method. ....8
Figure 2.2 Schematic of the cyclic immunofluorescence. ....9
Figure 2.3 Multiplex Co-fractionation/mass spectrometry workflow. ....11
Figure 2.4 Methods of fluorescence lifetime imaging microscopy. ....17
Figure 2.5 Physical properties of fluorophores. ....18
Figure 2.6 Linear unmixing of multiple fluorescent species on the phasor plot. ...21
Figure 3.1 Silica particle formation process via reverse microemulsions. ....34
Figure 3.2 Process of forming stable amide bond. ....35
Figure 3.3 Reaction between NHS and an amine group. ....36
Figure 3.4 Reaction for immunoconjugate forming. ....37
Figure 3.5 Calibration Curves of CZ QDs. ....42
Figure 3.6 DLS measurement of primary PEGylated silica particles with different amounts of MeTz. ....44
Figure 3.7 Optimization of backfilled PEG concentration. ....45
Figure 3.8 Effect of MeTz on particle size. ....46
Figure 3.9 Effectiveness of MeTz binding on silica surface. ....47
Figure 3.10 One-step staining on SKBR3. ....49
Figure 3.11 Two-step staining on SKBR3. ....50
Figure 3.12 Comparison of two staining methods. ....51
Figure 4.1 Size analysis of QDs in silica shells. ....58
Figure 4.2 DLS measurement of QDs with dark quencher in silica shells. ....59
Figure 4.3 Emission analysis of QDs in silica shells. ....61
Figure 4.4 Lifetime analysis of QDs in silica shells. ....62
Figure 5.1 DLS measurement of organic dyes in silica shells. ....69
Figure 5.2 Emission analysis of organic dyes in silica shells. ....70
Figure 5.3 Lifetime analysis of organic dyes in silica shells. ....72
Figure 5.4 Protection effect of silica shells. ....80
Figure 5.5 Lifetime comparison of probes in solution and on cells. ....82

# LIST OF TABLES

Table 5.1 Biomarker expression of four breast cancer cell lines. .....85

# LIST OF EQUATIONS

Eq. 2.1 ..... 20
Eq. 2.2 ..... 20
Eq. 2.3 ..... 20
Eq. 2.4 ..... 20
Eq. 2.5 ..... 20

# ACKNOWLEDGMENTS

I would like to express the deepest appreciation to my advisor and my committee chair, Professor Jered B. Haun. He is insightful and never loses his sense of humor. The completion of this study could not be possible without his expertise and guidance.

I want to thank my committee members Professor Michelle Digman and Professor Regina Ragan for their support and constructive feedback. I am grateful to Professor Stacy Copp and Professor Zhongping Chen for their scientific guidance.

Thank you to all the past and present group members who ever helped me or simply had nice talks with me. Luis Mejia, Xi Chen and Dr. Vanessa Herrera gave me the training on synthesis and purification techniques. I will deeply cherish the friendship and collaboration with Dr. Jinghui Zhao, Dr. Hauna Lagouros, Dr. Marzieh Aliaghaei and Kevin Lee. Gratitude goes to Alyssia, Veena and Jonathan for their assistance in this study.

I am grateful to the excellent scientists and engineers I've worked with. Special thanks to: Dr. Belén Torrado at Laboratory for Fluorescence Dynamic (LFD), Dr. Qiyin Lin at Irvine Materials Research Institute (IMRI), Dr. Adeela Syed at Optical Biology Core, and Dr. Dmitry Fishman at Laser Spectroscopy Laboratories. I want to thank LFD for providing facilities and technical support. I want to recognize NIH, NSF, Department of Materials science and Engineering and Department of Biomedical Engineering for their funding support.

Lastly, I want to express my heartfelt gratitude towards my family and friends. To my parents who I owe a lot, thanks for being my role models and supporting what I do. I am deeply appreciative of their sacrifices and unconditional love. To other family members and friends, thanks for always being there for me and inspiring me to be a better person.

# VITA

## Tingwei Deng

### EDUCATION

University of California, Irvine
Ph.D., Materials Science and Engineering 2024

Carnegie Mellon University
M.S., Material Science 2018

South China University of Technology
B.E., Polymer Science 2016

### JOURNAL PUBLICATION

1. **Deng, T.,** Lagouros, H.A., Haun, J.B. Developing Fluorescence Lifetime Libraries based on Silica Shells. *Manuscript In preparation.*

2. Naveen, V. Y., **Deng, T.**, Herrera, V., & Haun, J. B. (2023). Multiplexed immunoassay using quantum dots to monitor proteins secreted from single cells at near-single molecule resolution. *In Cancer Systems and Integrative Biology* (pp. 187-206). New York, NY: Springer US.

3. Lee, J., Wang, Z., Zhang, J., Yan, J., **Deng, T.,** Zhao, Y., ... & Bockstaller, M. R. (2020). Molecular parameters governing the elastic properties of brush particle films. *Macromolecules*, 53(4), 1502-1513.

### POSTER PRESENTATION

1. **Deng T.,** Zhao J., Haun J.B. (2022) Phasor Analysis of Fluorescence Lifetime Enables Quantitative Multiplexed Molecular Imaging of Three Probes. *UC System-Wide Bioengineering Symposium*. Poster presentation.

2. **Deng T.,** Haun J.B. (2024) Phasor Analysis of Fluorescence Lifetime Enables Quantitative Multiplexed Molecular Imaging of Three Probes. *Frontiers in Biological Fluorescence.* Poster presentation.

# ABSTRACT OF THE DISSERTATION

Developing Fluorescence Lifetime Probe Libraries based on Silica Shells

By

Tingwei Deng

Doctor of Philosophy in Materials Science and Engineering

University of California, Irvine, 2024

Professor Jered B. Haun, Chair

Breast cancer is the most diagnosed cancer in the world and is responsible for millions of deaths. Early-stage diagnosis enhances survival rates and extends life expectancy by enabling timely treatment interventions. Many cancer cell detection techniques have been developed, but lacking abundant probes limited their further application. The utilization of fluorescence lifetime and phaser plot approach makes it possible to push the limits. The fact that lifetime information exhibits in a semi phasor pixel by pixel makes detection easier and more convenient. However, developing suitable fluorescent probes for multiplexing is still challenging. Synthesizing new fluorescent species is time-consuming; additionally, it is hard to maintain a stable lifetime in a complex microenvironment. More importantly, the

number of probes strongly restricted the application of the technique. Multiplexing with 4-6 probes has been demonstrated, but the probe capacity needs to be further expanded. Therefore, fluorescent lifetime nanoprobes based on silica shells were proposed. Silica is biocompatible and surface modification versatile. Fluorescent species or their mixtures were wrapped within 30-50 nm silica particles. Because dye molecules inside the silica shells were so close to each other, the quenching effect could be utilized to change the lifetime of nanoprobes. In this study, I developed fluorescence lifetime libraries based on novel nanoprobes in silica shells for breast cancer cells detection. First, a method was shown to prepare silica particles modified with Polyethylene Glycol (PEG), where cell staining tests proved that the particles could specifically bind to cancer cells. Secondly, the fluorescence lifetime libraries were built with different fluorescent species. Through two approaches, addition of dark quencher and self-quenching, the lifetime of silica probes was altered, and the limit on number of probes was expanded. Lastly, a tumor panel was built and individual probe was validated on cancer cells, which proved the feasibility of using the silica probe for multiplexing. In summary, this study demonstrated that the fluorescence lifetime libraries using the innovative silica nano probes would serve as a powerful tool for multiplexing in breast cancer cells detection.

# CHAPTER 1 Introduction

Breast cancer is one of the most diagnosed cancers in the world, especially in developing countries. There are HER positive, ER/PR positive and triple negative breast cancer types. Triple negative breast center cells are not positive to HER2, ER and PR. Many scientists have been working on therapies to cure breast cancer. ER/ PR positive can be treated with hormone therapy, and antibody therapies are shown to be effective to HER positive breast cancers. However, no effective methods have been developed to treat triple negative breast cancer. Early-stage detection becomes essential for an increased survival rate.

Many techniques have been developed to detect cancers. The traditional immunohistochemistry uses antibodies to find antigens in tissues. Dual plex could be achieved; however, sample preparation is time-consuming, and the method gives false signals. Immunofluorescence has better sensitivity and stronger signal than immunohistochemistry, but the number of dyes used are limited. Though cyclic immunofluorescence allows more bio molecules to be detected, the sample preparation demands much effort and time. Mass spectrometry could detect molecules with low concentrations. M/z ratio is the base of mass spectrometry multiplexing. Conventional mass spectrometry used different isotopes as nanoprobes, and barcode amplification solves the problem of weak signal.

However, the attachment and detachment of barcodes are time consuming and so far, only enzymatic reactions are reliable. Mass spectrometry also requires large scale equipment, limiting its use. Another technique, flow cytometry, is limited by the probe number. The lack of spatial information, coupled with the challenges of resolving the whole spectra signal further limit flow cytometry. Hyperspectral imaging is a powerful tool for multiplexing, but it's complex and expensive. Extracting useful data from hyperspectral images is also challenging.

With the constraints of the varying techniques mentioned above, fluorescence lifetime imaging emerges as an alternative for multiplexing. Fluorescence lifetime is the time a fluorescent species stays in its excited state before it returns to the ground state, during which a photon is emitted. Usually, fluorescence lifetime is considered as the period when the intensity drops to 1/e of the intensity maxima. This lifetime is an intrinsic property of a fluorescent species, and it can be affected by external factors like pH, and temperature. Fluorescence quenching is any process that lower the fluorescence intensity of a molecule. Internal quenching is caused by factors like temperature and viscosity. The conformation of molecules is changed with the external factors. External quenching like FRET has some biomedical applications. During FRET, energy is transferred from donors to acceptors; for FRET to happen, the emissions of donors must overlap with the excitation spectra of acceptors, and they must be close to each other.

Fluorescence lifetime imaging microscopy (FLIM) has been developed to discriminate fluorophores and their unique structures. Through this technique the lifetime information can be gathered pixel by pixel. Two methods are used to capture lifetime using FLIM: time domain and frequency domain. The time domain approach uses fitting curve, whereas the frequency domain approach uses phase shift and amplitude variation. The amazing phasor approach makes it possible to transfer lifetime data onto a 2-D semi-circle, pixel by pixel. The pixels close to the origin point have a longer lifetime and those far from it have a shorter lifetime. What's more, the lifetime follows a linear principle. The lifetime of a mixture of two lies within the line connecting the two pure species, and the lifetime time of a mixture of three stays in the triangle of the three pure species. With FLIM and phaser plot, lifetime is used as multiplexing.

Silica nano particles are used in cell labeling and drug delivery. They have uniform particle size and large surface area. They are nontoxic, and easy to be modified. Because of those features, they have been widely used in biomedical applications. After being surface modified, they are excellent imaging probes and drug carriers. This was why silica particles were chosen in this study.

In this thesis, an innovative fluorescent silica particle probe was developed for detection of breast cancer cells. Libraries based on the silica particles were created for cancer diagnosis and research. The thesis starts with showing a method to

synthesize silica probes for cell labeling. Silica was made and modified with -COOH via reverse emulsion. The water-in-oil system was created because of surfactant. The hydrolysis of silicate was accelerated by ammonium. The silica shells were formed with fluorescent species inside. Primary PEG-24 and backfilled PEG8 were attached via covalent binding to promote hydrophily. It was later demonstrated that the silica particles could label breast cancer cells via specific binding. After proving the silica particles could be used as cell labeling probes, I successfully developed fluorescence lifetime libraries with two mechanisms. The lifetime of quantum dots was changed by adding dark quencher molecule in the QD library. Dark quencher took the energy emitted from QDs and release it as heat. While in the organic dye library, lifetime was adjusted by using different amounts of dye molecules. The energy was absorbed by the neighboring molecules and dissipated. The emission of the whole system was weakened, and the lifetime was shortened due to the quenching effects. Lastly, I created a tumor panel consisting of both QDs and organic dyes. The tumor panel included six probes and would be used to detect four breast cancer cell lines. Individual nanoprobes were validated on cells. In summary, the silica nanoprobes, with FLIM and phaser method, would be a powerful tool for cancer diagnosis.

# CHAPTER 2 Background

## 2.1 Breast cancer overview

Breast cancer is the most diagnosed cancer and a leading cause of death around the world. More than about 2.3 million new cases of female breast cancer were recorded in 2020 [1]. Most of the cases reported were found in developed countries because of the easier access to health care. It is believed that many cases were not reported in developing countries due to the lack of medical service and facility [2, 3]. The patients were not even diagnosed from the beginning, not to mention received treatment. With the fact that breast cancer places a burden on families and health systems, it is vital not only to study tumor formation and heterogeneity, but also to come up with effective ways of diagnosis and therapy of breast cancer.

The use of biological markers provides accurate diagnosis of breast cancer and increases patient survival. Depending on the expression or not of molecular markers for hormone (estrogen or progesterone) receptors and human epidermal growth factor 2 (HER2), breast cancer is categorized into three major subtypes [4]. They are hormone receptor positive (70% of cases), HER2 positive (15%-20%) and triple negative (15%). And systemic therapy for nonmetastatic breast cancer depends on these subtypes. Hormone receptors positive patients are treated with

endocrine therapy [5]. HER2 positive tumors receive HER2-targeted antibody or smaller molecule inhibitor treatment [6]. Triple-negative breast cancer (TNBC), which is the most aggressive subtype, is lack of hormone receptors and does not overexpress HER2 [7, 8]. Compared with the other two subtypes, TNBC has shorter survival time, higher mortality rate and higher recurrence rate. Traditionally, chemotherapy and immunotherapy are applied to treat them, and some new methods like noncoding RNA [9] has been proposed. However, side effects like weakening immune systems, low specificity, especially high recurrence rate are still an issue. Therefore, many studies have been working on finding effective ways to diagnose TNBC at an early stage. And the precision and effectiveness of biomarkers in breast cancer diagnosis highlight the need for further development and utilization of these valuable tools.

## 2.2 Molecular multiplexing techniques

### *2.2.1 Immunohistochemistry*

Immunohistochemistry (IHC) is a conventional method for tumor detection. IHC uses antibodies to detect antigens in a tissue and look for signs of abnormal in it [10, 11]. Tissue samples obtained from a biopsy are frozen or fixed and sectioned into slices, then antigen retrieval techniques are used to expose and restore antigenicity. The samples are subsequently treated by blocking agents [12]

like serum protein or bovine serum albumin (BSA), then primary antibodies and secondary antibodies are applied to the samples. The presence of the target proteins is observed through the enzymatic conversion of a substrate at the binding sites. IHC can spatially localize and quantify the biomarkers in a tissue [13, 14]. It's been proved that IHC has good indication for ER [15], PR [16], Ki-67 [17] and HER2 [18] biomarkers. However, IHC has some limitations. IHC can only detect one biomarker at a time, which is called singe plex. Usually, more than one biomarker is needed to diagnose one cancer type. The sample preparation is time consuming. What's more, it may give false-positive or false-negative results, depending on how the tissue samples are treated in different labs [19, 20]. The quality of antigen, antibodies, and the reaction between them affect the accuracy of the results. The concentration of antibody expression also affects the results. High concentration causes saturation, which affects the detection accuracy [21, 22]. Many studies have been conducted to push the staining limit of IHC. Dual plexed IHC was reported; brown DAB chromogen is used to label one target and red chromogen is used for the other one. These dyes were used for CD3/CD20 dual staining in immune cells [23], and AMACR/p63 prostate tumor detection [24]. Though duplexing is easy to execute, it has issues like false signal due to colocalization, and the limitation of usable antibody species.

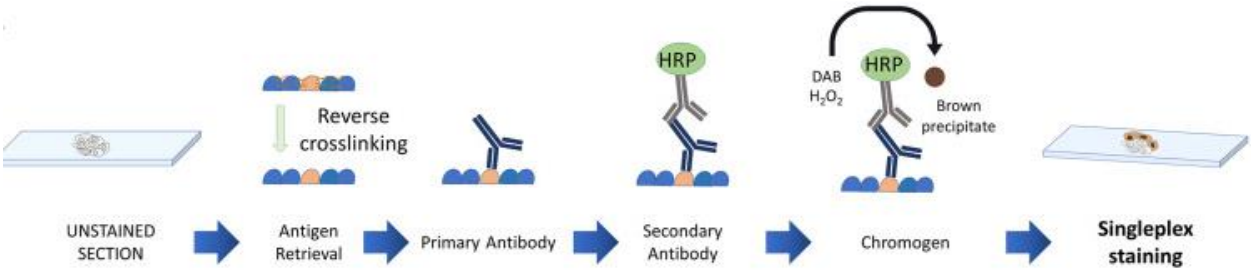



**Figure 2.1 The workflow for chromogenic immunohistochemistry using the indirect method.** The sectioned sample is stained with the primary antibody, which is detected by a species-specific secondary antibody conjugated to enzymes, such as one or multiple horseradish peroxidase (HRP). [25]

### *2.2.2 Immunofluorescence*

Immunofluorescence (IF) is an important technique for localization, detection and pathway studies in different tissues [26, 27]. IF has excellent sensitivity and allows signal amplification comparing to IHC. The final antibodies are conjugated with fluorophores that are excited by a specific wavelength and emit lights with longer wavelength due to energy loss. Multiplex immunofluorescence (mIF) tyramide signal amplification is a new tool for cancer detection [28]. This technique starts with antibody selection. A panel of primary antibodies of interest are validated. Then the antibodies are conjugated with different labeling fluorophores, which have same excitation but different emission spectra. Alexa fluor dyes [29] and Cyanine dyes [30] are commonly used. The

conjugated antibodies are incubated with treated tissue samples with blocking agents. After the unbound conjugates are washed away, the tissues are mounted in slides and are ready to be image under fluorescent microscopes. This technique has high sensitivity and spatial revolution. However, the number of the dyes are limited because of the range of UV-vis wavelength [31]. The emission spectra start to overlap if 4-5 dye conjugate or probes are applied, making it hard to distinguish among them. Cyclic Immunofluorescence (CyCIF) allows more biomolecules to be detected [32]. The samples are first stained with several fluorescent dye conjugated antibodies. After the signals are collected, the fluorophores are photobleached and washed away. Then a new set of fluorescent dye conjugated antibodies are added. However, using CyCIF is time consuming [33]. The samples may degrade over time and the fluorescence signals from previous cycles may interfere the following rounds [34], which cause false positive results.

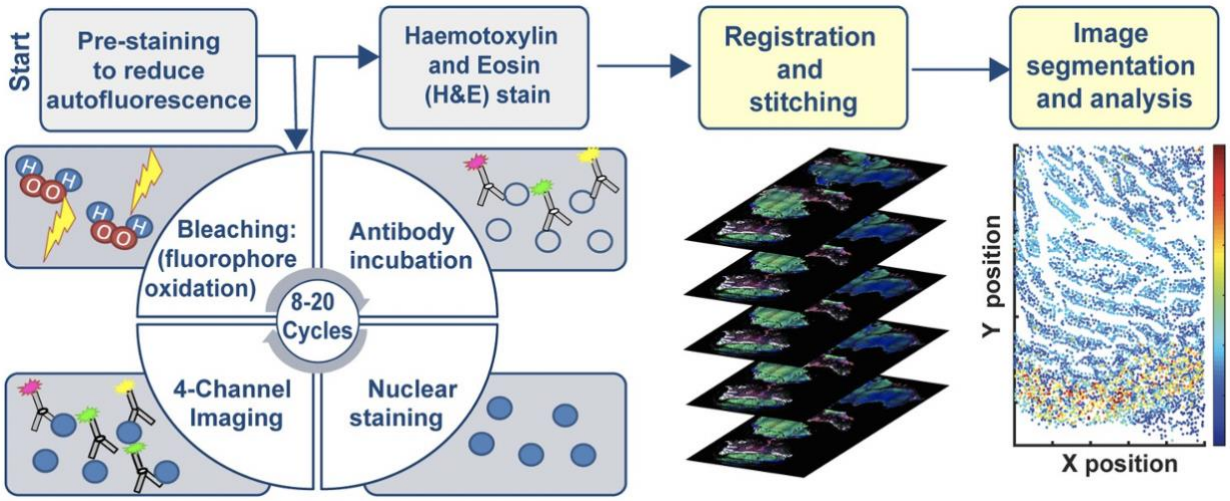



**Figure 2.2 Schematic of the cyclic immunofluorescence.** Tissue images are assembled via multiple rounds of four-color imaging. [32]

### *2.2.3 Mass Spectrometry*

Mass Spectrometry (MS) is a mass-based determination approach that can discriminate many biomolecules with low concentrations. Most elements [35], many biomarkers [36] can be tested by diffident type of mass spectrometry. The m/z ratio is the base of this MS [37], so the design of mass-tag probes is important. Conventional MS multiplex uses different isotopes as nanoprobes. UV light or ion beam are applied, and mass spectrometry signals are collected [38, 39]. Barcode amplification is used for advanced mass spectrometry [40, 41]. In this case, a mass tag consists of recognition region and barcoding region. The recognition region is connected to a bio molecule through a specific interaction such as base pair hybridization [42], enzyme-substrate [43] or antigen-antibody reaction [44]. And

the barcoding region is vital for signal transformation. The recognition and barcoding regions of a mass tag are connected via a linker so that the mass tags can be released easily by some triggers [45, 46]. The workflow of using MS for multiplexing starts with preparing mass tags, which are subsequently added to target molecules. That follows with incubation and unbound mass tags washing. Lastly the barcoding regions are detached and used for analysis. Many types of mass tags have reported, such as metal isotopes [47] and nanoparticles [48]. Stable isotope Lanthanide (Ln) ions are used because they can connect with macrocyclic chelating agents [49]. Hu et al. [50] developed dual aptamer-functionalized gold nanoparticles for SMMC-7721 and A549 cancer cell detection. However, multiplex mass spectrometry has some disadvantages [51]. First, the number of isotopes is limited. And the isotopes that can be modified to let the attachment and detachment happen are even fewer. What's more, the existing amplification methods restricted the use of MS. Only enzymatic reactions and nano particles have been used to amplify signals. Lastly, MS multiple depends on larger-scale instruments, which many labs cannot afford. Portable devices are needed to expand the use of this technique.

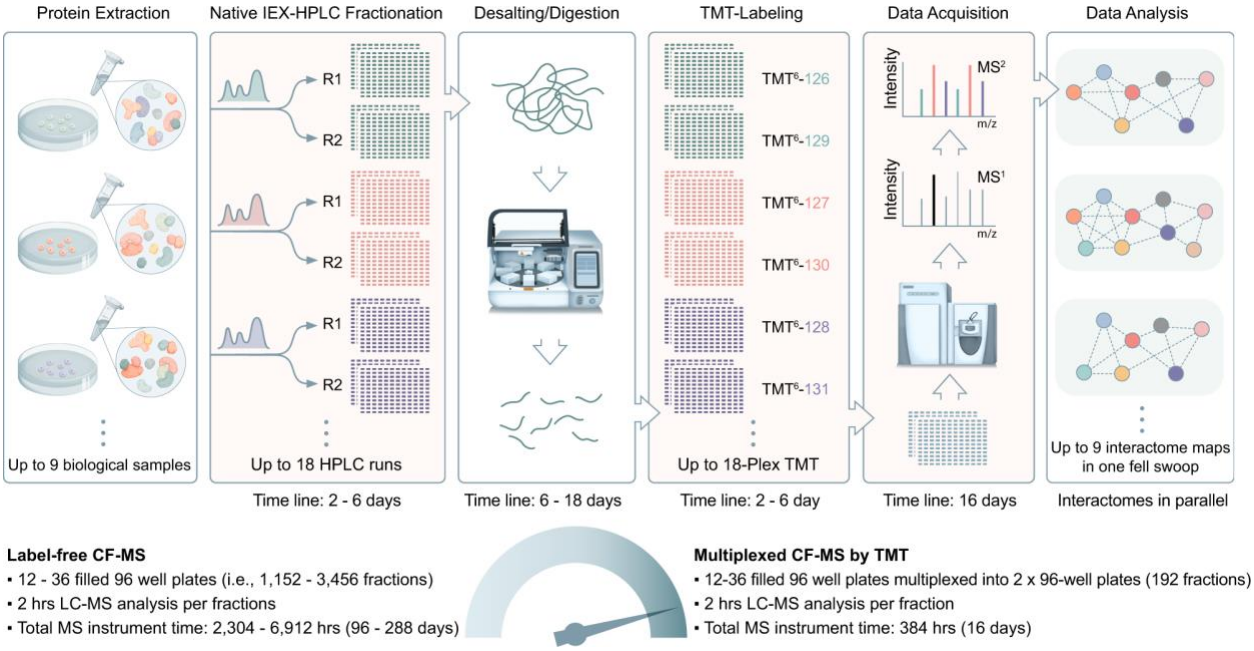



**Figure 2.3 Multiplex Co-fractionation/mass spectrometry workflow.** Main modular steps of CF/MS [52]: 1. native protein extraction; 2. biochemical fractionation (replicates R1/R2); 3. automated protein desalting and digestion; 4. isobaric tandem mass tag (TMT) labeling; 5. LC/MS data acquisition; 6. data analysis.

### *2.2.4 Flow Cytometry*

Flow Cytometry (FCM) is a sophisticated technique for biomarker classification and molecule analysis, utilizing light scattering and fluorescence emission. The technique has evolved with the effort of different studies, such as fluorescence microscope [53] and the use of fluorophore conjugated antibodies [54]. The combination of flow technology and fluorescence really paved the way for FCM to be applied to almost all aspects in biologicals, from small molecule discovery [55] to cell sorting [56]. Briefly, cells and particles are prepared in a suspension and are labeled with fluorescent dye conjugated antibodies. The

antibodies are used to label specific antibodies of biomolecules. Next, a sample is injected into a flow cytometer and gets excited by lasers. The lasers emit lights with different wavelengths. The scatter and fluorescent signals are detected and collected by optical components. Forward scatter and side scatter signals are used to measure cell size or granularity and internal complexity or granularity, respectively. And both provide the information of morphology and structure. Multi-channel of fluorescent emissions enables multiplexing detection of labelled cells. The scattering and fluorescence information are acquired for each individual cells, allowing identification [57] and quantification analysis [58]. However, FCM for multiplexing has some limitation. The number of probes is restricted. While polychromatic flow cytometry can use different detectors to collect signals from different single fluorochrome, only a portion of one signal can be collected and this portion contain signals from other fluorochromes [59]. Spectra Flow Cytometry focuses on the whole spectra signal instead of individual fluorochrome, but it's challenging to unmix the spectra signal for analysis [60]. And the spatial information of tissues is missing. Because the samples are prepared in suspension, FCM can't be used for those who are interested in cell distribution or localization.

### *2.2.5 Hyperspectral Imaging*

Hyperspectral Imaging (HSI) gather images where single pixel is related to a full spectrum [61, 62]. Spectral and spatial features are combed to create a 3D data cube. Unlike multispectral techniques, HIS enable to provide information of via a continuous spectrum, allowing expand the information storage [63]. The range of a spectrum is not limited to visible light, HIS can reach up to near-infrared range (400-1000 nm) [64]. HIS system has potential for non-invasive tumor detection. After light is applied, the information such as refection [65], fluorescence [66] or transmission [67] are detected for tumor cells diagnose and pathological studies. Samuel et al. [68] reported a customized hyperspectral imaging system with deep learning neural network to detect breast cancer cells. Besides high dimension of information, HIS has high resolution. However, HSI is complex and expensive [61, 62]. Advanced sensors and analysis tools are required. Data processing is another problem [69]. Extracting useful information from the data is really challenging, owing to its vast amounts of spectrum information. Noise reduction, calibration and sophisticated algorithms are necessary [61, 70].

## 2.3 Fluorescence Lifetime Imaging Microscopy and Phasor Approach

### *2.3.1 Fluorescence Lifetime and Quenching*

Fluorescence lifetime is defined as the time a fluorescence specie stays in its excited state before emitting a photon and returning to its ground state [71, 72]. And the fluorescence lifetime ($\tau$) of a molecule is considered as the time interval when the intensity drops to $1/e$ of the maxima after it is excited [73]. When a simple fluorophore absorbs a certain amount of energy, photophysical phenomena such as internal conversion and fluorescence happen. Intersystem crossing and phosphorescence happen in a more complex system. The fluorescence lifetime is an intrinsic character that is determined by the chemical structure of a molecule [74]. Molecule concentration, and measure method don't affect the fluorescence lifetime. External factors like temperature [75], pH [76] and polarity [77] can alter the fluorescence lifetime of a molecule by affecting the photophysical events. On one hand, designing a stable fluorophore is important for molecule and biomarker labeling considering the complexity of the tissue samples. On the other hand, altering the lifetime with different approaches leads to new applications in molecule detection. Among the commonly used fluorophores, organic dyes have

lifetime between 0.5 to 4 ns, while quantum dots exhibit lifetime in the range of 10 to 100 ns [78, 79].

Fluorescence quenching is defined as any process that lower the fluorescence intensity of a molecule samples [80]. There are internal quenching and external quenching [78]. As for internal quenching, environmental factors such as temperature [81], viscosity [82], and polarity [83] change lifetimes by changing the conformation of a molecule. Excited state charge transfers such as electron transfer (ESET), proton transfer (ESPT) and intersystem crossings are structurally related instead of environmental factors [84]. External quenching includes FRET [73], Dexter Electron transfer [85], Dynamic quenching [86]. Forster Resonance Energy Transfer (FRET) with lifetime is a powerful technique to study molecule structures, molecule interaction and cell-cell interaction. For FRET to occur, donor emission spectra should overlap with acceptor absorption spectra, and the donor and the acceptor must be within certain distance [87].

### *2.3.2 Fluorescence lifetime imaging microscopy*

Fluorescence lifetime imaging microscopy (FLIM) has been applied to identify fluorophores and their unique structure [88]. FLIM measures lifetime of a fluorophore in a pixel-by-pixel manner and distinguishes the variations of fluorophores with similar spectra [89]. For example, free and bound NADH can be

easily detected using FLIM [90]. FLIM is used in tumor detection and drug delivery. Lifetime measurement using FLIM can achieved by either time-domain or frequency-domain measurements [91]. Time-domain approach measures the exponential decay of a fluorescent molecule after it is excited by a short pulse light [92]. The photon counts are collected continuous and are made into a histogram. And a fitting curve is later applied to calculate the lifetimes. Alternatively, frequency-domain approach uses the phase shift and the amplitude variations between a periodically modulated excitation signal and a emission signal [93]. The excitation signal is considered as a sinusoidal wave. The exponential decay of the fluorescence intensity is quantified by the phase delay and amplitude modulation.

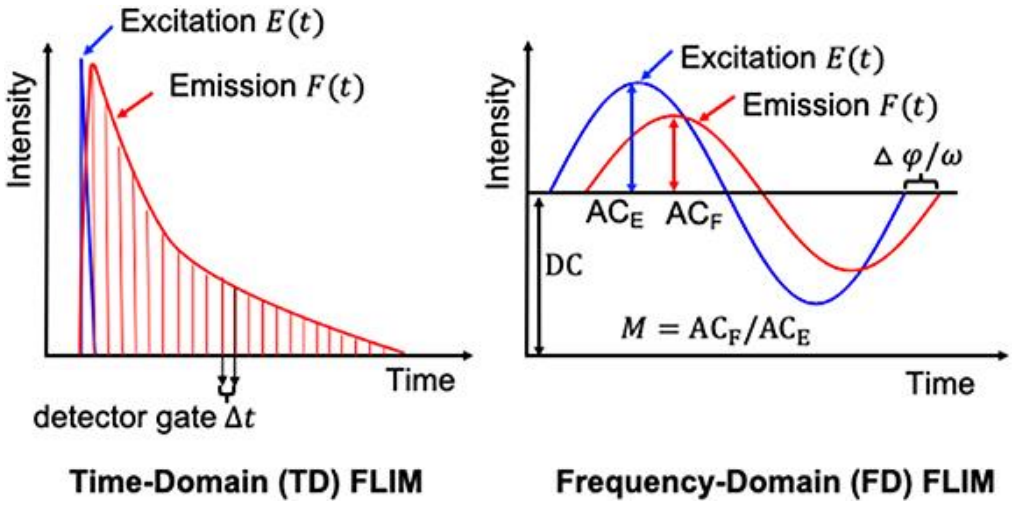



**Figure 2.4 Methods of fluorescence lifetime imaging microscopy.**
$E(t)$ and $F(t)$ are the excitation and emission signals, respectively. Left: time-domain FLIM implemented with time-gating; $\Delta t$ is the duration of the time gate, respectively. Right: frequency domain FLIM; $AC_E$ and $AC_F$ are the AC parts of the

excitation and emission signals; $M$ and $\Delta\varphi/\omega$ are the modulation degree change and phase shift, respectively, of the emission with respect to the excitation.[94]

### *2.3.3 Phasor approach to FLIM and Linear combination*

The phasor approach to FLIM simplified the image analysis by transferring data, pixel by pixel, onto a two-dimension phasor plot [95-97]. Finding a curve to precisely fit the exponential decay is challenging. Using the correct curve fitting model to analyze fluorescent molecules with multiexponential decay or a mixture of molecules is even harder [95]. In the phasor approach, the fluorescence decay of each pixel is exhibited simply in a semi-circle phasor. Single exponential decay is located on the universal circle, while multi-exponential decay is located inside the circle. The pixel close to (0,0) has longer lifetime, while the pixel close to (1,0) has shorter lifetime.

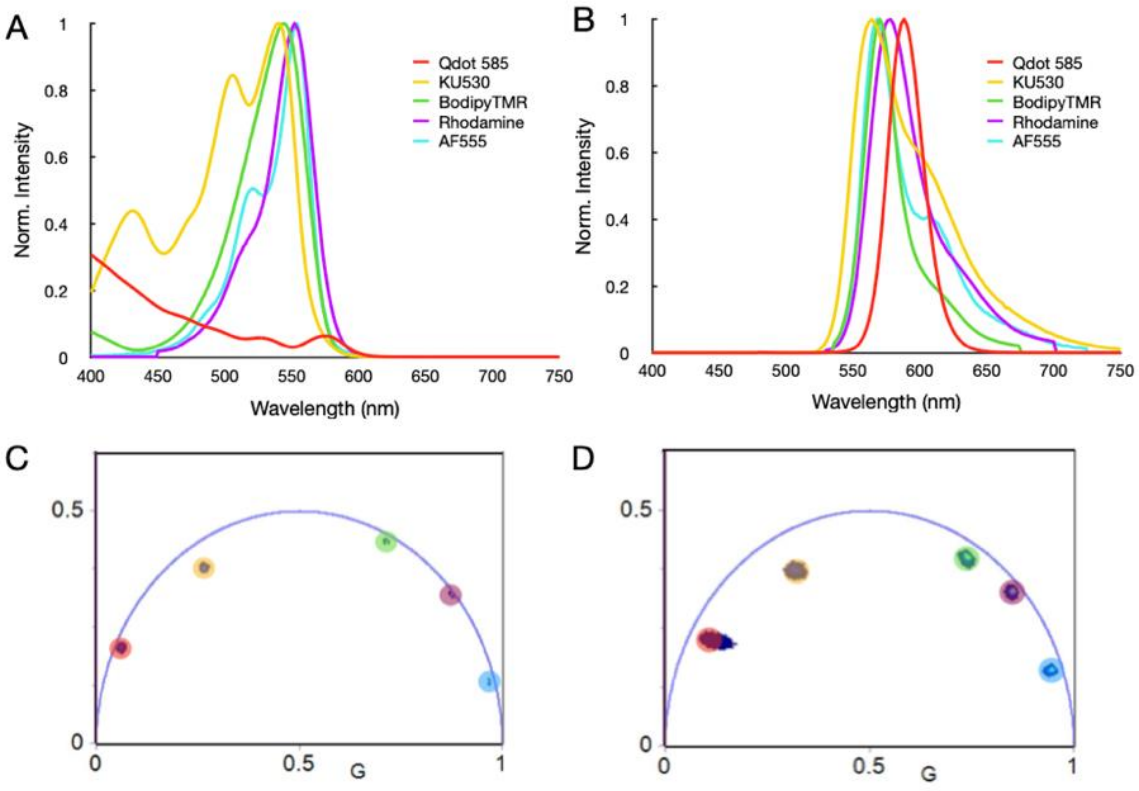



**Figure 2.5 Physical properties of fluorophores.** Spectral properties of fluorophores Qdot585, KU530, BodipyTMR, Rhodamine and AF555 were shown in (A) excitation spectrum and (B) emission spectrum. Lifetimes of fluorophores in solution (C) or on cells (D) were tested. Reference to Haun lab.

The mathematical correlation between emission signals and phasor of each pixel are shown in the following equations [98]. Eqs. 2.1 to 2.3 are applied to transform lifetime in time-domain to phasor space. i and j are X and Y coordinates of a pixel of the original image, $I_{i,j}(t)$ is the intensity decay. $g_{i,j}(\omega)$ and $s_{i,j}(\omega)$ are the X and Y coordinates in the phasor plot. $\omega$ is the angular repetition frequency ($\omega$=2$\pi f$) of a laser. T is the interval between two pulses and $I_0$ is the

max intensity. Eq. 2.4 and 2.5 are applied in frequency-domain, where $m_{i,j}$ and $\varphi_{i,j}$ are modulation and phase shifts at each image pixel.

$$g_{i,j}(\omega) = \int_0^T I_{i,j}(t) \cdot \cos(n\omega t)\, dt \Big/ \int_0^T I(t)\, dt \qquad \text{Eq. 2.1}$$

$$s_{i,j}(\omega) = \int_0^T I_{i,j}(t) \cdot \sin(n\omega t)\, dt \Big/ \int_0^T I(t)\, dt \qquad \text{Eq. 2.2}$$

$$I(t) = I_0 \cdot e^{-t/\tau} \qquad \text{Eq. 2.3}$$

$$g_{i,j}(\omega) = m_{i,j} \cdot \cos(\varphi_{i,j}) \qquad \text{Eq. 2.4}$$

$$s_{i,j}(\omega) = m_{i,j} \cdot \sin(\varphi_{i,j})$$

The phasor follows the linear combination principle [99, 100]. In a two-component system, the lifetime of a mixture is in the line connecting the lifetime clusters of these two pure species. And the lifetime of a mixture of three species are in the triangle connecting the lifetime clusters of these three pure species. The distance of the mixture to a pure specie is inversely related to the fraction contribution of the pure specie. The closer the mixture lifetime is to a pure specie, the bigger fraction this specie contributes. Either two or three component has algorithms to reveal the information with only one harmonic [98]. Unmixing the information of systems with more than three components involves more harmonics [99]. Technically speaking, phasor approach can be expanded to the resolve any

number of components and polygons with extra harmonic frequencies, which makes phasor FLIM method a powerful tool for high order molecular analysis.

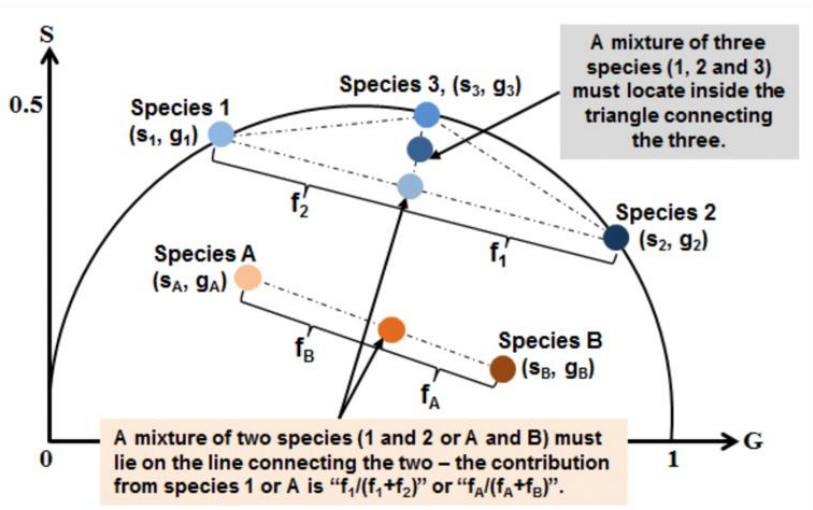



**Figure 2.6 Linear unmixing of multiple fluorescent species on the phasor plot.** The lifetime of a mixture of two exhibit in the line connecting these two pure species, while the lifetime of a mixture of three shows in the triangle connecting these three. [99]

## 2.4 Nanoparticles

### *2.4.1 Nanoparticle and its application*

Nanoparticles are important in the development of nanotechnology because of its variable applications in different fields. Nanoparticle is defined as a particle with a size between 1 to 100 nanometers [101]. Nanoparticles exists in nature and are important in the earth system [102], like bassanite in sea water, iron Oxide in iceberg sediment, manganese oxide in umber. Human studies, makes and uses

nanoparticles in different fields, like metal binding [103], water pollution absorption [104] and cancer treatment [105]. According to what nanoparticles are made of, nanoparticles are categorized into inorganic and organic nanoparticles. Organic particles are formed by polymers like polypeptides [106] or polyethylene glycol [107] and are widely used in biological applications[108, 109]. They are usually biodegradable, nontoxic and sensitive to factors like temperatures or pH, which makes them a really good carrier for drug delivery. The most famous case is the application of covid vaccines [110]. The RNA is stored in the lipid micelles and later injected into the human body. More research has been conducted to study the potential use of those lipid particles for HIV and cancer vaccines [111]. Inorganic particles have a variety of applications depending on the materials. Metal/ metal oxides nanoparticles have distinct properties from their bulk forms, making them a useful tool for developing clean energy and building a low carbon environment [112]. They have high surface area to volume ratio, pore size, surface charge and surface charge density, crystalline and amorphous structures. Nickel oxide and gold nanoparticles are good catalyst carriers for hydration and carbon capture [113, 114]. Adding small amounts of transitional element nanoparticles into metal can give unexpectedly excellent property improvements [115]. Carbon based nanoparticles have good thermal and electrical properties [116], and they are widely used in semiconductor manufacturing. These particles have excellent

properties and are appliable in the industry, but they are toxic and not suitable for biological purposes. Silica particles, on the other side, are biocompatible and nontoxic [117], making them a good media for drug delivery and fluorescence labeling for cancer diagnoses.

### *2.4.2 Silica particle*

Silica, or silicon dioxide, is commonly found in nature. As the matter of fact, silica is the most common mine, known as quartz, in the earth crust and takes of 10% of its mass [118]. Human use of silica traces back to thousands of years ago across different civilizations. Egyptians used silica to create glassware and glass ornaments [119]. Roman constructed buildings with silica rich materials [120]. And china has a long history of making delicate potteries out of silica [121]. During the industrial revolution, the demand for silica surged due to the manufacturing of glass and ceramics. With the emergence of nanotechnology and deeper understanding of nanoparticles in the late 20th century and the early 21st century, silica on a nanoscale gained much attention, especially in therapeutic/diagnostic applications, because they are biocompatible, have large surface areas and their surface can be modified easily. Silica is “Generally Recognized As Safe” (GRAS) by the FDA, and is widely used in cosmetic products and as food additives [122].

The presence of silano groups provide silica nanoparticles uniform pore size, controllable particle size, large surface area and easily modified surface [123, 124]. There are mainly two types of silica nanoparticles: Nonporous and mesoporous silica particles [125]. Nonporous silica particles have rigid surface and show excellent biocompatibility. They are widely used in encapsulation systems for imaging and drug delivery [126]. Mesoporous silica particles have special structures, like large surface area, high thermal stability, and controllable porosity, which makes them an ideal carrier for drug release systems [127].

Many methods have been developed to produce silica nanoparticles [117]. Aerosol route burns SiCl4 in an oxygen-rich hydrogen gas flam reactor and requires high temperatures [128]. In acid precipitation method, alkali metal silicate is reacted in an acidic environment to produce silica particles [129]. This method happens in room temperature but the process of removing salt and purifying the particles is time consuming. The Stober synthesis [130] were used to make silica particles by adding alcohol, or other organometallic silicon precursor via hydrolysis. And then the sol-gel silica is centrifuged, washed, and dried. Improved Stober synthesis have been developed to get specific particle sizes, surface modification porosity and surface area. The microemulsion synthesis generates silica nanoparticles in water-in-oil within microemulsions [131, 132]. Surfactants, which have both hydrophobic and hydrophilic functional groups, form

microemulsions in the water-in-oil system. The alkyl silicate slowly diffuses into the system and moves from oil phase to water phase, where hydrolysis happens. The base catalysis, for example, ammonia, promotes the process. The surfactants are removed and the microemulsion is terminated by organic solvent like ethanol. The microemulsion synthesis is size and morphology controllable, versatile in surface functionalization and timesaving. Most importantly, the water-in-oil system can be adapted to encapsulate dyes or drugs, which makes this method widely used for making silica particles in therapeutical and pharmaceutical applications.

### *2.4.3 Biomedical applications of silica nanoparticles*

Silica particles have been used for biomedical purpose because of their excellent biocompatible properties. They are commonly used in drug delivery [133, 134]. The drugs are firstly encapsulated or attached to the silica particle surface. When the particles reach a specific part of a body, the drugs are released under stimulus such as pH or temperature. The nanoparticle for drug delivery and therapy requires surface modification [135, 136]. Carboxyl (COOH) [137], phosphonate ($CH_3HPO_2$) [138], poly (ethylene glycol) (PEG) [139], and amine (NH2) [140], poly peptides [141] and copolymers [142] have been used for modification. Those polymer chains form ‘brush’ structure on the surface of the

particles, thus makes the particles more hydrophilic [143]. The repulsive force among the particles keeps them from aggregating and keeps the proteins and other molecules away from the particles. Wiesner et al.[144-147] invented microdots named C dot with a size of 6 nm for cancer treatment, which were approved by FDA for human clinical trials on gastric cancer. C dots were modified by PEG and targeted target HER-2. And they could carry five times more drugs than most of the antibodies. A biodegradable zinc ion coated silica particles were reported to be toxic to breast cancer cells not to healthy epithelial cells or murine macrophages [148].

Drugs are applied during the synthesis or post absorption[133, 149]. The advantage of post loading is the additional step allows optimization of drug loading. There are two main types of stimuli: internal and external [150]. Internal stimuli are cause by the difference between healthy and abnormal cells or tissues. For example, the microenvironment of cancer cells tends to have lower pH than the normal ones and thus can be a stimulus for drug release [151]. Magnetic field, ultrasound and light are the common examples of external stimuli. For example, two photon absorptions are used to deliver reactive oxygen species, drug and even genes to kill cancer cells [152].

The other biomedical application of silica particles is early diagnoses or bio imaging [153]. Finding an effective way to detect cancers at an early stage is the

main goal for nanomedicine. Many techniques like superparamagnetism, fluorescence, and absorption have been developed over the past few decades [154]. However, those techniques have limitation like fast degradation and difficulty of surface modification for targeting. And silica nanoparticles are a promising agent for bio-imaging and have many advantages [117]. First, the silica shell is chemically stable and protect the fluorescent dyes from degrading on various physiological conditions like pH and temperatures. At the same time, toxic fluorophores could be applied with the nontoxic silica shells. What's more, silica capsulates large amounts dyes, which increases imaging contrast or high signal-to-noise ratio. Last, silica particles are easy to be modified and stable in various circumstances. Many fluorophores that are synthesized in hydrophobic solvent could be used with the silica shells.

Like drug delivery, organic dyes, quantum dots, carbon dots or upconversion nanoparticles are encapsulated within or conjugated with silica shells. Heidegger et al. [155] reported fluorescein isothiocyanate (FITC) conjugated silica particles to trace T and B cells. The particles were later modified with polyvinylpyridine (PVP) and showed a speckled distribution pattern of fluorescent signals within dendric cells. Mohamed et al. [156] synthesized core shell CuInS2/ZnS QDs embedded silica particles for cancer cells diagnose. The quantum dots showed a red shift on emission after silica shells were added. Gao et al. [157] prepared Fe3+

nano sensors with silica doped carbon dots to detect cancer cells. Liu et al. [158] constructed NaYF4:Tm/Yb/Gd upconversion nanoparticles with silica shells applicable for NIR and MRI dual imaging. Silica particles are used for different techniques like Magnetic Resonance Imaging (MRI), Positron Emission Tomography (PET) and Computed Tomography (CT) as a probe and usually combined with drugs for detection and treatment at the same time. Ma et al. [159] developed Au silica particles as contrast agent, which showed a noticeably darker MR contrast. Chen et al. [160] prepared silica particles with 64 Cu and TCR105 together with human/murine chimeric IgG1 monoclonal antibody for targeted imaging. Chen, Peng, et al. [161] synthesized FePt nanoparticles modified with polydopamine as CT contrast agent. The silica layer enhanced PDA-Fe3+ loading and improved contrast. In summary, with its excellent bio properties, silica particles have great promise in cancer diagnose, biomarker detection and drug delivery.

### *2.4.4 Quantum dots basic*

Quantum dots are a kind of semiconductor with sizes of several nanometers (4 to 12 nm in diameter) [162]. Since their first discovery in the 1980s, quantum dots have gained great interest due to their excellent optical properties [163]. They attract large attention in molecule tracking [164], fluorescent labeling [165] and

drug delivery [166]. The optical features of quantum dots root from quantum confine effects [167]. When the size of a semiconductor particle becomes smaller than the exciton Bohr radius, the motion of charge carriers (electrons and holes) become confined and leads to discrete energy levels instead of continuous energy bands. When a quantum dot absorbs energy that is larger than its bandgap, electrons are excited into the conduction band from the valence band. The electrons subsequently move back to the valence band and emit a photon. Compared to organic dyes, quantum dots have broad excitation range, narrow excitation spectra, a high quantum yield and higher stability over time. Importantly, because of the bandgap, the emission wavelength is adjustable by tuning the size of the quantum dot. Larger quantum dots have smaller band gaps, emit smaller amounts of energy, making the emission wavelength longer. While smaller quantum dots have larger band gaps and emit higher energy photons.

Quantum dots are categorized into 12 types according to the composites they are made of [168]. Conventional quantum dots consist of two parts [169]: a heavy metal core and a semiconductor shell. The core is usually made of II–IV, IV–VI, or III–V semiconductors like CdTe, CdSe and PbSe. And the shells are ZnS or SiO2, which increase quantum yield. Zhang et al. [170] reported photoactivated CdTe/ CdSe quantum dots as NIR fluorescent probe to detect biothiols, which provide

good sensitivity and selectivity for detecting cysteine, homocysteine, and glutathione. Yin et al. [171] developed PbS quantum dot photodetectors for NIR with high sensitivity. Despite all the advantages of quantum dots, they are toxic for cells and tissues due to the leaching of Cd ions from the cores, which restricts their application in biological purposes.

To overcome the issue of toxicity, many studies have been conducted. One way is to prepare toxic ion free quantum dots[172]. Chen al et. [173] made InP quantum dots for light applications. Park al et. [174] reported silica quantum dots that can be excreted from the body. ZnS quantum dots attain much attention because of their stability[175], large retention capability[176], and lower amounts usage of polluted reagents via easy synthesis[177]. ZnS also has a high surface area to volume ratio, which makes it a good nano-photocatalyst [178, 179]. With newer studies, more nontoxic quantum dots have been reported.

The other way is to modify the surface of the toxic quantum dots or to add a shell to prevent the inner ions from leaching. Many methods have been reported, among which are surface ligand-exchange[180, 181] and coating of biocompatible materials like silica [182, 183] or polymers [184]. During the process of surface ligand exchange, the hydrophobic ligands on the surface, for example, trioctylphosphine oxide (TOPO) [185], are replaced by hydrophilic ones like 2-aminoethanethiol [186] to improve water solubility of quantum dots. Even though

the solubility is improved after the ligand exchange, the physicochemical properties of the quantum dots surface and quantum efficiency may be affected [187]. Encapsulating the quantum dots with silica is the most preferred approaches to improve biocompatible and stability. Tetraethyl orthosilicate (TEOS) is used to form the silica surface coating of quantum dot and enhance water solubility. Specially, silanes with functional groups, such as aminopropyl silanes[188], phosphor silanes [189], and polyethylene glycol(PEG)-silanes [190] are added during the silica shell growth for further modification. All these new development makes quantum dots a good choice for bioimaging.

# CHAPTER 3 Developing Nanoprobes with Silica Shells

## 3.1 Introduction

Breast cancer threatens people's life and place heavy burden on millions of families, so it's important to diagnose cancer at an early stage to save lives. It is studied that early diagnosis with proper therapy can increase survival rate over five years. Among all probe technologies, silica particles have been studied and developed because of its biocompatibility and modification versatility. Silica particles is nontoxic and compatible with issues and cells, making it a perfect vehicle for fluorophores. What's more, micro reverse emulation method is a

convenient approach for making silica encapsulated particles in room temperature. However, silica particles tend to aggregate and got stuck with cells via nonspecific binding. Therefore, surface modification is necessary to make the surface more hydrophobic and thus prevent nonspecific binding. PEG has been studied and used for silica modification due to its biocompatibility and chemical availability. Specifically, using both primary pegs and back filled pegs effectively prevents aggregation and nonspecific bindings.

In this chapter, I will report a synthesis method for preparing the silica probes. CdSe/ZnS quantum dot was used. Briefly, silica particles with quantum dots were prepared via reverse emulation. And subsequently particles were modified with long primary PEGs, followed with short back filled PEGs. First, the primary PEGylation was optimized and the effect of MeTz was studied. Then, the back filled PEG was optimized. Lastly, the specific binding of the silica probes was tested by staining breast cancer cells via HER2.

## 3.2 Materials and Methods

### *3.2.1 Materials*

Cyclohexane, (3-Aminopropyl) triethoxysilane (APTS), IGEPAL-CO520 surfactant, Tetraethylorthosilicate (TEOS), Ammonium hydroxide (30% in water), 3-(Trihydroxysilyl) propyl methylphosphonate (TPMP) were purchased from Sigma-Aldrich (St. Louis, MO). Carboxyethylsilanetriol (CEST) was purchased

from Gelest (Morrisville, PA). Methanol and Ethanol purchased from Sigma-Aldrich (St. Louis, MO). Amicon Ultra Centrifugal Filter (100kDa) was purchased Millipore Sigma (Burlington, MA). CdSe/ZnS quantum dots (CZ) 580nm was purchased from NN Crystal (Fayetteville, AR). CdSe/CdS quantum rods, 590nm peak emission was purchased from Strem (Newburyport, MA). Dark quencher QXL 570 acids, SE was purchased from AnaSpec (Fremont, CA). Methyltetrazine-PEG24-amine, methoxy-PEG24-amine and methoxy-PEG8-amine were purchased from BroadPharm (San Diego, California). N-(3-Dimethylaminopropyl)-N'-ethylcarbodiimide hydrochloride (EDC) and N-Hydroxy succinimide (NHS) were purchased from Sigma-Aldrich (St. Louis, MO).

### 3.2.1 Modification of Organic dyes or Dark Quencher

1.28 moles of organic dyes/dark quencher were reacted with the equivalent amount of APTS in ethanol, so that the dyes/dark quencher was silanized and was included in the silica particles. The reaction time was 24 hours at room temperature. This step was skipped if no organic dyes or dark quenchers were used.

### *3.2.2 Preparation of Silica Particles via Reverse Microemulsion*

The reaction was optimized to use 1.3 mL IGEPAL-CO520 surfactant within 10 mL of cyclohexane in a 20 mL glass vials. Sonicated for 1 min. Next, organic dyes or quantum dots were added, sonicated for 5 mins. 150 μL ammonium

hydroxide was added, followed by sonicating for 1 min. Finally, 80 μL of TEOS was added and allowed to react for 24 hours at room temperature to produce silica particle shells. The silica shells were further modified with carboxylic groups and phosphonate groups were attached to improve dispersibility. 4 μL of Carboxyethylsilanetriol and 2 μL of 3-(Trihydroxysilyl) propyl methylphosphonate were added, followed with 24 hours reaction at room temperature.

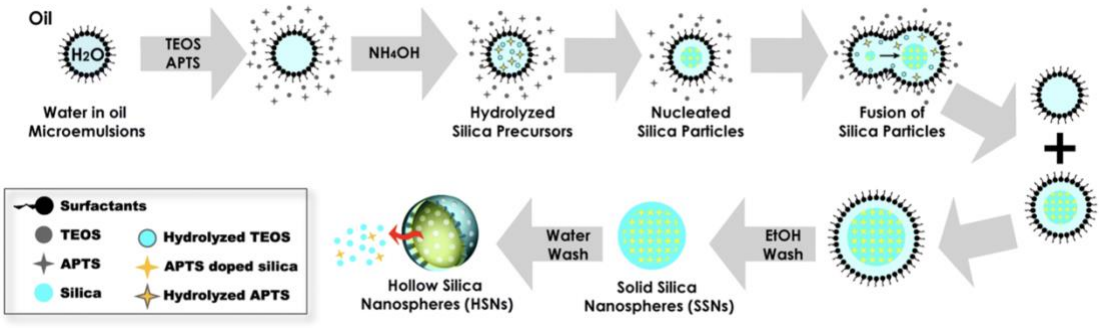



**Figure 3.2 Silica particle formation process via reverse microemulsions.** Surfactants form the 'water in oil' system. Silica is formed in the water phase by the hydrolysis of TEOS. The reaction is stopped by washing. [190]

Washing step was applied to terminate the rection and remove excess reagents. Synthesis was mixed with 0.5 volume equivalents of Methanol, followed with vortex. The mixture was centrifuged at 15000 rpm for 20 min. The supernatant was removed. The pellets were dissolve with 50% of ethanol by sonicating. The dissolved solution was transferred into an Amicon filter, followed by centrifuging. The particles were purified in 50% ethanol two times, followed with water one time. The particle samples were stored in water at 4 °C.

### *3.2.3 Primary PEGylation of Silica Particles*

Polyethylene glycol (PEG) was selected due to its biocompatibility and immune-compatibility, and hydrophicity. Methyltetrazine-PEG24-amine (MeTz-PEG24) and methoxy-PEG24- amine (mPEG24) reacted with the carboxylic groups on the silica shells with N-(3- Dimethylaminopropyl)-N-ethylcarbodiimide hydrochloride (EDC) and N-Hydroxy succinimide (NHS). Reacting with EDC crosslinker, carboxylic acid formed an unstable o-Acylisourea intermediate. The presence of NHS further helped form a stable amide bond. After 3 hours, the synthesis was transferred into a 100kDa Amicon filter for purification, followed by three times of wash with water. The particle samples were stored in water at 4 °C.

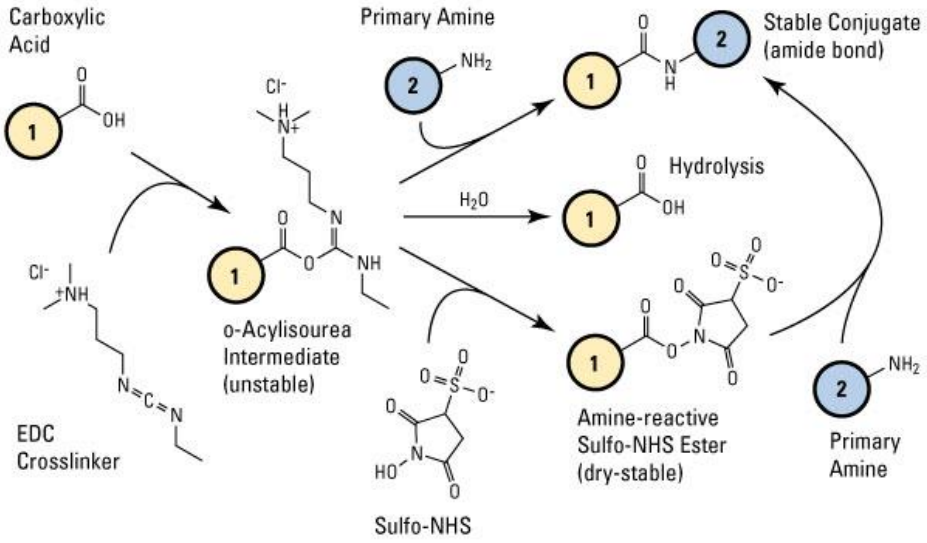


**Figure 3.4 Process of forming stable amide bond.** The amines of carbodiimide EDC crosslinks react with carboxylic acids to form unstable intermediates. Sulfo-NHS increases the yield of the stable conjugates [191].

### *3.2.4 Backfilled PEGylation of Silica Particles*

Similar to primary PEG modification, methoxy-PEG8- amine (mPEG8) were conjugated onto the carboxylic group of the primary PEGylated silica particles with EDC and NHS. After 3 hours, the synthesis was transferred into a 100kDa Amicon filter for purification, followed by three times of wash with water. The particle samples were stored in water at 4 °C.

### *3.2.5 Antibody Modification*

The chemical biomarker hyphenate strategy, that antibodies of interest were modified with TCO and used to couple with MeTz-modified nanoparticles onto live cells, was reported [191].

Briefly, HER2 antibody, which is overexpressed in SKBR3 cell line, was modified with TCO-NHS ester, by the reaction between amine groups and NHS ester.

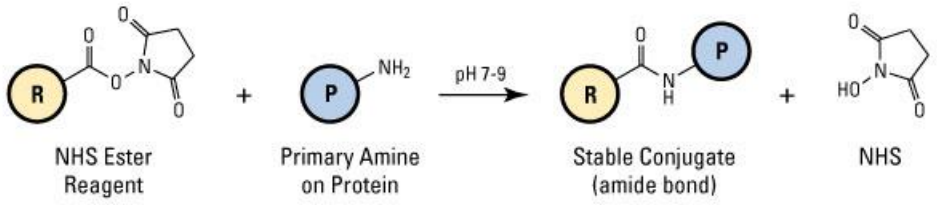



**Figure 3.6 Reaction between NHS and an amine group.** NHS ester reacts with an amine on protein to form a stable conjugate. [191]

200 µg of HER2 antibody was reacted with 30 mole equivalents of NHS-TCO in PBS+ (PBS with 1% BSA) with 10% total volume of DMF and sodium bicarbonate (0.1M, pH=8.4) at room temperature for 3 hours. Modified antibody was purified by 40K ZebaTM Spin Desalting Column. The concentration of the recovered sample was measured by absorption measurements using NanoDrop.

### *3.2.6 Immunoconjugation*

Immunoconjugates were prepared with MeTz-PEGylated nanoparticles and 30x TCO-modified HER2 antibodies. MeTz-PEGylated particles and 10 mole equivalents of 30 x TCO-HER2 were added into PBS+ (PBS with 1% BSA), followed with 1 hour of incubation. The conjugates were purified by HPLC. The immunoconjugates were collected and concentrated with 100kD Amicon centrifugal filters. The conjugate samples were stored at 4 °C.

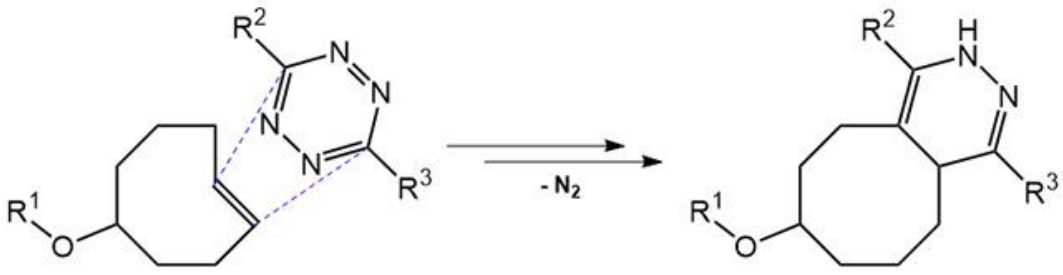



**Figure 3.8 Reaction for immunoconjugate forming.** Diels-Alder cycloaddition reaction between a trans-cyclooctene (TCO) and a tetrazine, followed by a retro-Diels-Alder reaction under elimination of N2 [193].

### *3.2.7 Cell Culture and Cell labeling*

SKBR3 cell line was maintained in McCoy's 5A 1x base media, supplemented with 10% FBS, 1% Pen/Strep and 1% L-glutamine. Cells were incubated at 37 ºC and supplied with 5% CO2.

Cells were plated in 8-well microscope chambers 2-3 days prior to imaging and made sure the cell confluency reached 75~80% when used.

The cells were washed with PBS+ one time to remove the media. For one-step staining, cells were directly stained by immunoconjugates and incubated for 20 mins. For two-step staining, cells were first stained by TCO-modified HER2 antibodies at 10 μg/mL for 30 mins, followed by adding MeTz-modified silica particles for 20 mins. The incubation process was conducted at room temperature, and after each incubation step, cells were washed with PBS+ to remove excess antibodies or immunoconjugates. Later 200 μL of PBS+ was added into each cell well for imaging.

Stained cells were imaged by a confocal microscopy (Leica TCS SP8, Optical Biology Core Facility at UCI). Samples were excited at 405 nm, and the emission between 588-635 nm was collected.

### *3.2.8 Techniques*

Many techniques were used to test the particle samples and the labeling cells. The immunoconjugate were purified by a AKTA Pure Chromatography system. The analysis included dynamic light scattering (DLS) to determine probe size with a Malvern Zetasizer Nano DLS system, fluorometry with a Tecan Spark multimode microplate reader, absorbance with a Nanodrop, scanning electron microscopy (SEM) with a FEI Magellan 400 XHR system, transmission electron microscopy (TEM) with a JEOL-2100F, fluorescence confocal microscopy with a Leica TCS SP8. The details of the equipment are shown below.

**AKTA Pure Chromatography System:** the AKTA Pure is a broad-range purification system that can be configured for a variety of applications, for example, size exclusion chromatography. It is equipped with two high-precision pumps, each with two inlet valves, as well as a mixer to deliver multiple buffer solutions and generate gradients. Additionally, the conductivity monitors with built-in temperature sensor measures conductivity of buffers to ensure the delivery of true gradients. The UV/Vis monitor can detect absorbance at up to three wavelengths in 190-770 nm range, ensuring precise sample monitoring and protein separation. The accompanying UNICORN software enables intuitive system control and automation for reproducible purification. This equipment is available in Haun lab.

**Malvern Zetasizer ZS Nano DLS:** the Malvern Zetasizer Nano DLS is a two-angle particle analyzer utilizing dynamic light scattering with non-invasive backscatter (NIBS) optics to perform significantly better than 90 degree scattering systems. Nano DLS is used extensively for size and zeta potential measurements of nano-scale particles and colloids. Size measurements may range from 0.3 nm to 10 μm in diameter with concentrations as low as 0.1 ppm. Nano DLS also enables the measurement of protein mobility and molecular weight. This equipment is available in the Laser Spectroscopy Laboratory at UCI.

**Tecan Spark multimode microplate reader:** the microplate reader has High Speed Monochromator. It offers full absorbance spectrum from 200 to 1000 nm, excellent accuracy in the deep UV range (230-260 nm), and an OD range from 0-4 that ensures good linearity, requiring fewer dilutions and less manual pipetting. This equipment is available in Copp Lab at UCI.

**FEI Magellan 400 XHR SEM:** the FEI Magellan 400 XHR SEM scanning electron microscope capable of to support flexible imaging operations and refined topographic and materials information. The 5 axis piezoceramic Magellan stage allows for a wide travel range in a highly adaptative and large chamber. Both small and large samples can be positioned under the beam in virtually any orientation. Wide field optics allows for an electron beam resolution as high as 0.8 nm at 15 kV

and 1.5 nm at 200 V. This equipment is available at the Irvine Material Research Institute (IMRI) at UCI.

**JEOL-2100F TEM:** JEOL-2100F TEM is equipped with a Schottky type field emission electron source, providing accelerating voltage up to 200 kV. The 2.8 mm focal length in the cryo-pole piece permits the acquisition of tomographic data with a maximum tilt angle up to ±80°. JEM-2100 is equipped with both Gatan K3 direct electron detector and Gatan Oneview camera. K3 camera carries a large collection area (5760 x 4092 pixels) and a fast collection rate at 1500 frames per second. Gatan OneView CMOS camera is also installed on 2100F for routine screening and acquisition of high contrast images/diffraction patterns with a field of view at 4k x4k pixels. OneView carries a high dynamic range (more than 16bits) and "live" experience with 25 frames per second at full image resolution. The equipment is available at the Irvine Material Research Institute (IMRI) at UCI.

**The Leica TCS SP8 confocal microscopy:** the system has been designed for confocal microscopy with optimal photon efficiency and high speed. This system has 4 detectors (2 GaAsP and 2 PMT), 6 laser lines (405, 458, 488, 514, 568, and 633) and a motorized stage. There is a 10x air objective, 20x multi-immersion objective, and 63x oil objective with a very large field of view (comparable to 40x). The equipment is available at the Optical Biology Core Facility (OBC) at UCI.

**Fluorescence Lifetime Imagen Microscopy (FLIM):** M1 and Alba are customized for confocal microscopy and lifetime measurement. M1 has 2 laser lines (350 and 514) and a motorized stage. The pulsed laser frequency is 20 MHz. Alba system has a pulsed white light laser at 80MHz with a motorized stage. The equipment are available at the Laboratory for Fluorescence Dynamics (LFD) at UCI.

### *3.2.9 Calibration curve for CZ QDs concentration*

The stock CZ quantum dots solution was diluted into different concentration. The absorbance at 350, 400 and 450 nm were measured by NanoDrop. Three calibration curves were created. When an absorbance signal was measured, the solution was calculated with three curves. The final concentration is the average of three.

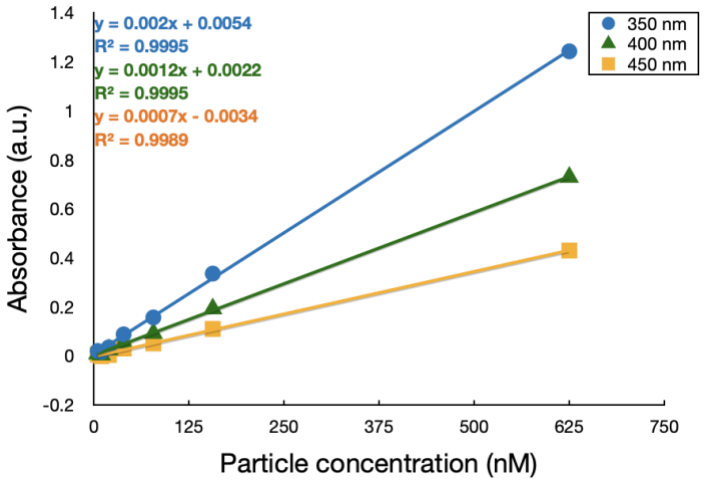


**Figure 3.10 Calibration Curves of CZ QDs.** The absorbance of CZ quantum dots was measured at 350, 400, and 450 nm. The concentration was the average of the concentrations calculated by the three wavelengths.

## 3.3 Results and Discussion

### *3.3.1 Tetrazine effect in Primary PEGylation*

In order to prevent aggregation and enhance biocompatibility, PEG was applied to the surface. Several linkers were reported by our lab for PEG attachment, for example, Azido and DBCO. After several experiment, the idea of using Methytetrazine-PEG-amine (Tz-PEG) was put forward to modify silica particles. m-PEG24 and MeTz-PEG24 were used for primary PEGylation. 100 μM of primary PEGs, including m-PEG24 and MeTz-PEG24, were used. The molar ratio of primary PEG: EDC: NHS was kept 1:3:0.9, according to preliminary tests. That said, the concentrations of primary PEG, EDC and NHS were 100, 300 and 90 μM, respectively.

The effect of primary PEG was tested by using 0%, 3% and 10% of MeTz-PEG24, shown in table 1. The silica particles were stable in both water and PBS. The particle size increased after PEG was attached. What's more, the amount of concentration of Methyltetrazine didn't significantly affect the size of the particles, with all being under 30 nm. Therefore, the concentration of Methyltetrazine barely

had effect on the particle size, which enable the tunability of concentration for tetrazine-PEGs for cell staining.

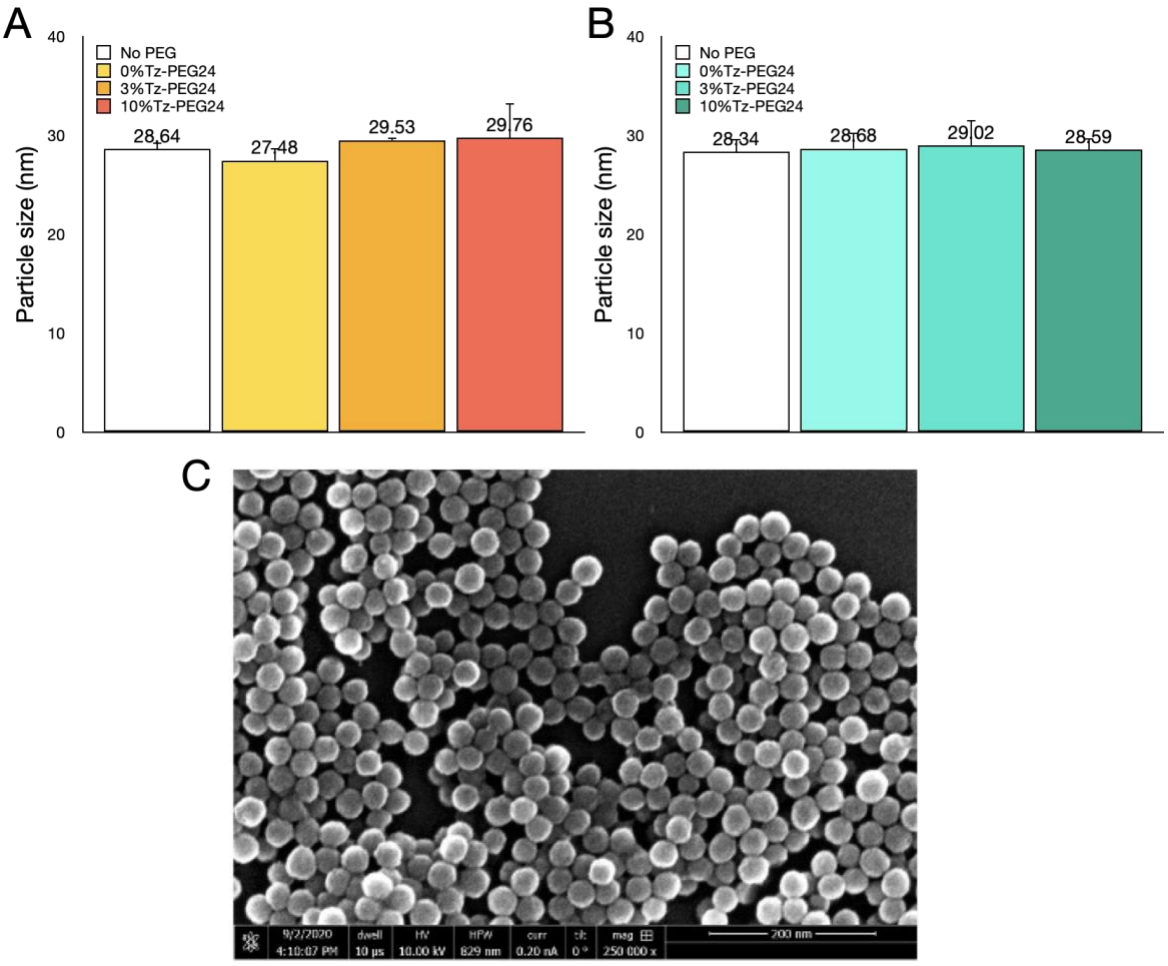



**Figure 3.12 DLS measurement of primary PEGylated silica particles with different amounts of MeTz.** The particles were measured in water (A) and PBS (B). TEM image shows size of non-modified particles (C). Silica particles were modified with 0, 3 and 10% of MeTz-PEG24. Non-modified particles were used as reference.

### *3.3.2 Backfill PEGylation Optimization*

mPEG8-amine was used as backfill PEG to prevent small molecules trapping among primary PEGs on the surface of silica shells. The sizes measured by DLS were shown in figure 3.7. Similarly, different concentrations of backfill PEGs were used to modify the silica surface, and corresponding concentrations of EDC/NHS coupling were added. The molar ratio of backfill PEG: EDC: NHS was 1: 3: 0.9, based on our previous study. Non-PEGylated particles (No PEG) and primary PEGylated only silica particles (mPEG24 only) were used as controls.

The sizes of particles were below 50 nm in diameter in water. The particles exhibited the smallest size at a concentration of 100 μM in water, and at a concentration of 300 μM in PBS. Some of the unreacted PEGs were adhesive to the surface of the of silica shells via non-covalent connection. With the attachment of PEG8, those impurities trapped within PEG24 chains were pushed away, which resulted in the decrease of particle size. However, when more mPEG8 was added, the extra PEG8 chains gathered and stuck on the silica surface, which led to the particle size increase. 100 μM was the optimal concentration and would be used for backfilling PEGylation in the further studies.

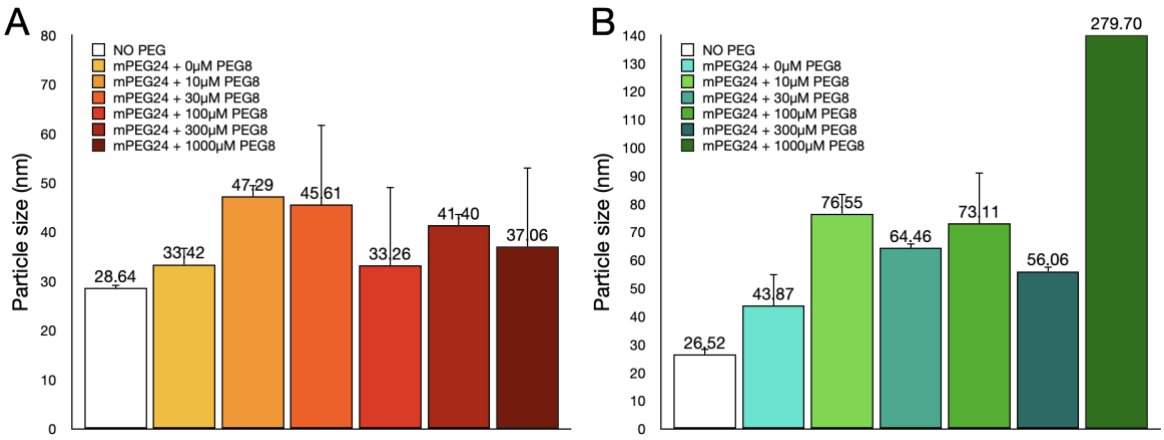



**Figure 3.14 Optimization of backfilled PEG concentration.** The particles were measured in water (A) and PBS (B) by DLS. Silica particles were modified with 100 µM of mPEG24 and later 0, 10, 30, 100, 300 and 1000 µM of mPEG8. Non-modified particles were used as reference.

The effect of Methyltetrazine (MeTz) in PEGylated silica particle size was studied. The silica particle was modified with 100 µM PEG24 and 100 µM mPEG8. Different percentages of MeTz were used. From the results in Figure 3.8, it is confirmed that the particle size remains similar regardless of the various amounts of tetrazine. And the existence of MeTz made the particles slightly smaller.

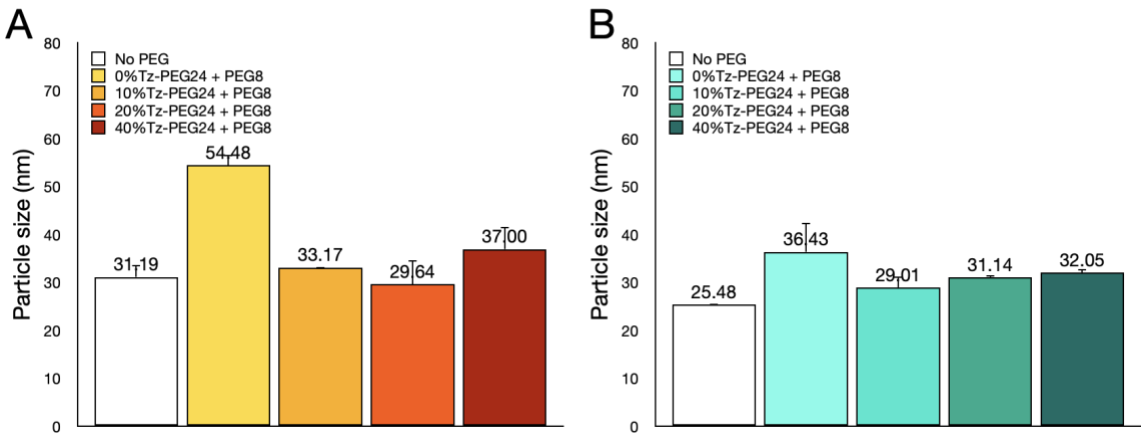



**Figure 3.16 Effect of MeTz on particle size.** PEGylated silica particles were measured in water (A) and PBS (B) by DLS. Silica particles were modified with 100 μM of mPEG24 and 100 μM of mPEG8. 0, 10, 20, 40 % of MeTz-PEG24 were used. Non-modified particles were used as reference.

The effectiveness of MeTz binding of particles was confirmed by conjugating excess of TCO-Cy5 with PEGylated particles. The same concentration of PEGylated particles with different percentages of MeTz were reacted with 10 moles equivalent of TCO-Cy5. After 1 hour of incubation, excess Cy5 dyes were washed with water four times by 100kD Amicon Centrifugal filters. The absorbance of Cy5-conjugated particles was measured by NanoDrop at 650 nm to avoid the interference of CZ signal. The absorbance results demonstrated that higher percentage of MeTz showed stronger Cy5 signals. And the difference in sample color further proved different amounts of dyes were conjugated to particles. 0% MeTz particles showed yellow color, and 20% MeTz particles exhibited blue.

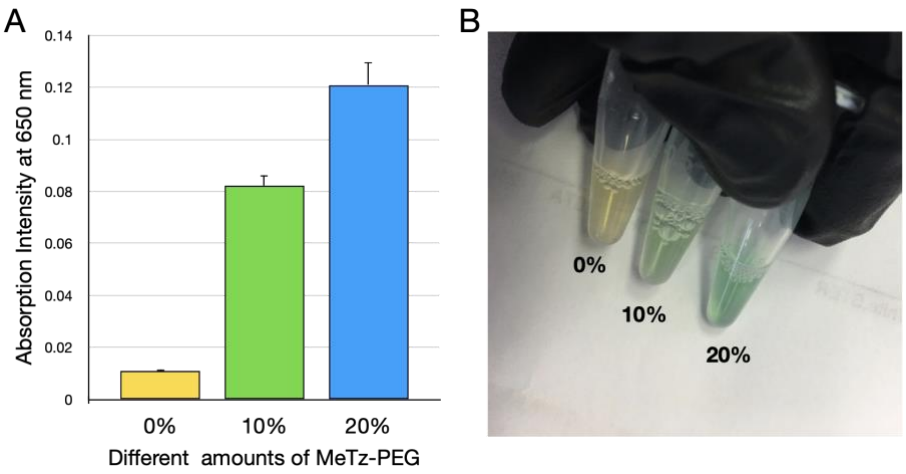



**Figure 3.18 Effectiveness of MeTz binding on silica surface.** The absorption intensities of particle-Cy5 (A) were measured at 650 nm. The color of solutions (B) further proves the effective of MeTz. 0, 10 and 20 % of MeTz-PEG were used to modify the silica particles.

### *3.3.3 Cell Staining to determine Specific Bindings*

After being optimized, the PEGylated nanoprobes were applied to HER2 positive SK-BR-3 breast cancer cells for labeling. Both one-step staining and two-step staining were conducted. Antibody-particle conjugates were prepared and directly added to cells in a one-step staining process, while in a two-step staining process, cells were first stained with modified antibodies followed by the addition of particles.

For one-step staining, 2, 5 and 20 nM of HER2-particle immunoconjugates (IC) were used to stain SK-BR-3 cells, with 20% MeTz. No treatment (autofluorescence) cells were used as control. Cells were stained with different concentrations of IC and washed after incubation. Cells without treatment were

washed by PBS+. And all the cells were in PBS+ while the images were captured by fluorescence confocal microscopy, shown in Figure 3.10. The cell surface was stained by the conjugates. The cells treated with particles directly showed lower signals than those stained with IC, which proved that the conjugates were attached to cells via HER biomarkers. Interestingly, particles were not fully washed away and were aggregated. However, as the particle concentration increased, the intensity rises of IC exceeded that of particles without antibodies, resulting in an enhanced contrast between IC and its counterpart. The intensity of IC was three times larger than its counterpart at concentration of 20 nM. Therefore, it was demonstrated that the silica particles were able to attach to the HER2 biomarker by one-step staining.

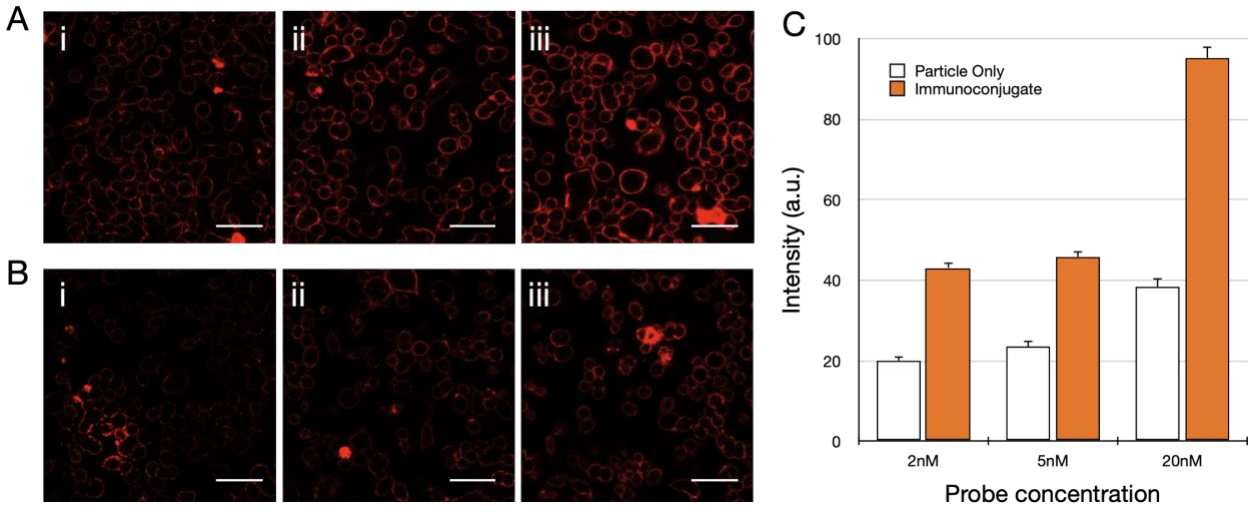



**Figure 3.20 One-step staining on SKBR3.** Cells treated by immunoconjugate (A) and particle (B) were imaged by a confocal microscope. 2nM (i), 5nM (ii) and 20nM (iii) of 20% MeTz PEGylated particles were used. The intensities (C) were calculated by ImageJ. Non treated cells and cells treated by particles without HER2 were used as controls. Scale bar is 1 mm.

For two-step staining experiment, 20, 50 and 70 nM of silica nanoprobes were used to stain breast cancer cells, with 20% MeTz. Cells were first treated with and without HER2 antibodies and were stained with different concentrations of particles. Cells without treatment were washed by PBS+, as control. And all the cells were in PBS+ while the images were captured by fluorescence confocal microscopy, shown in Figure 3.11. Cells with HER2 antibodies showed higher signals than those without HER2 antibodies, which demonstrated that the particles were conjugated to the cell surface thorough HER2 biomarkers. Therefore, it was proved that the particles were attached to the HER2 biomarkers by two-step staining successfully.

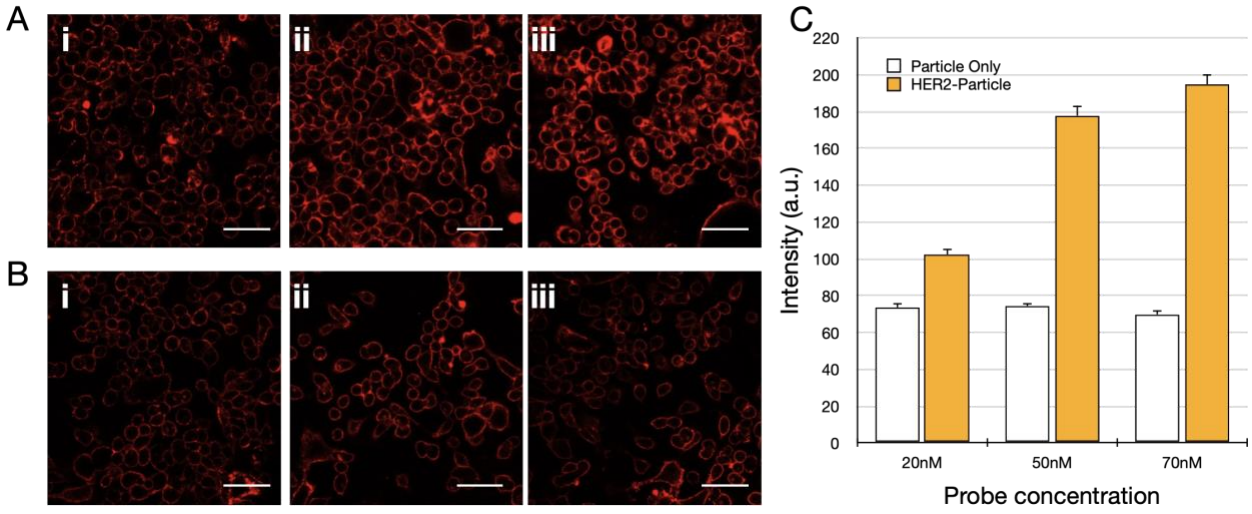



**Figure 3.22 Two-step staining on SKBR3.** Cells treated by HER2-particle (A) and particle (B) were imaged by a confocal microscope. 2nM (i), 5nM (ii) and 20nM (iii) of 20% MeTz PEGylated particles were used. The intensities (C) were calculated by ImageJ. Non treated cells and cells treated by particles without HER2 were used as controls. Scale bar is 1 mm.

Additionally, the efficiency of one-step and two-step staining were compared. Cells were stained with the same particle concentration by one-step and two-step methods. Cells stained by IC showed higher signal than those treated via two-step approach. It showed that one-step staining had a higher efficiency than two-step process.

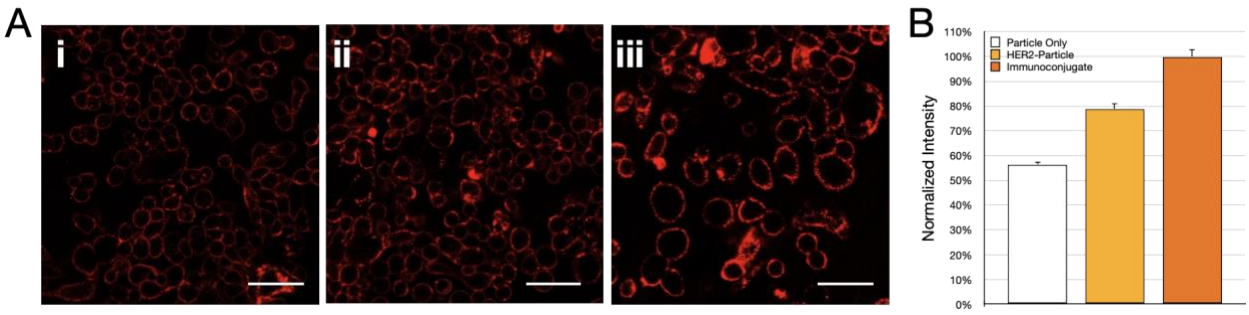



**Figure 3.24 Comparison of two staining methods.** Confocal images of cells (A) treated by particle (i), HER2-pareticle (ii) and IC (ii) were captured. 20nM of 20% MeTz PEGylated particles were used. The intensities (B) were calculated by ImageJ. Non treated cells and cells treated by particles without HER2 were used as control. Scale bar is 1 mm.

## 3.4 Conclusions

In conclusion, the silica nano probes were successfully prepared and optimized. Using CZ quantum dots as an example, the silica particles were synthesized via reverse emulsion. The sizes were within 30-50 nm, confirmed by DLS images. It was confirmed that adding more MeTz-PEG enabled probes have

more binding sites. And the percentage of MeTz doesn't change the particle size. What's more, the ratio of EDC/ NHS coupling, primary and backfilled PEGs concentration were optimized. Last and the most important, it was proved that the silica particles were able to stain breast cancer cells via specific bindings. Therefore, the silica shells could serve as a vehicle for different fluorescent species. And lifetime libraries could be built by encapsulating different species into the silica shells.

# CHAPTER 4 Measuring Lifetime of Quantum dots with Silica Shells using FLIM

## 4.1 Introduction

Fluorescence lifetime is a property of fluorescent molecules or quantum dots that are utilized to distinguish fluorescent species. Traditional, emission signal has been used to differentiate different species because it's straightforward and easy to measure. However, the usable UV-Vis wavelength range can only fit 5-6 distinguishable spectra. Emission spectra is broad and overlap if too many are used. Lifetime provides an alternative for fluorescent species differentiation. Fluorescence lifetime is termed as the time it takes for an excited molecule to

move from its excited state to ground state. Energy is released as light if photons are released. Species with similar emission spectra can have totally different lifetimes. Utilizing fluorescent lifetime expands the number of detection probes. Next, phasor approach displays the lifetime of a confocal image pixel by pixel. The lifetimes were presented in a semi phasor according to lifetime and complexity. Species with single exponential pulse show on the outer circle while complex species display inside the semi-circle. And linear combination rules are used for bio applications like detection of NADH/NAD+.

It was proved that five or six fluorescent species with different lifetimes were able to multiplex. However, the species number were still limited. That was why we wanted to build a fluorescent lifetime library, with which we could have plenty of probe candidates. And encapsulating those fluorescent species into a small silica particle made lifetime manipulation possible. The dye molecules were so close to each other that quenching effects became obvious. Quenching shortened lifetimes and weaken the emission because energy emitted was transferred to another species or dissipated as heat.

In this chapter, I will present the fluorescent lifetime libraries with quantum dots and darker quencher. In the quantum dot library, the lifetime was adjusted by addition of dark quencher. Firstly, all the quantum dots probes were synthesized. And dark quencher was added to mix with quantum dots. Secondly, the sizes were

measured by DLS and TEM. The emission spectra were measured and analyzed. Last, the lifetime was measured and the QD lifetime library was built.

## 4.2 Materials and Methods

### *4.2.1 Materials*

Cyclohexane, (3-Aminopropyl) triethoxysilane (APTS), IGEPAL-CO520 surfactant, Tetraethylorthosilicate (TEOS), Ammonium hydroxide (30% in water), 3-(Trihydroxysilyl) propyl methylphosphonate (TPMP) were purchased from Sigma-Aldrich (St. Louis, MO). Carboxyethylsilanetriol (CEST) was purchased from Gelest (Morrisville, PA). Methanol and Ethanol purchased from Sigma-Aldrich (St. Louis, MO). Amicon Ultra Centrifugal Filter (100kDa) was purchased Millipore Sigma (Burlington, MA). CdSe/ZnS quantum dots (CZ) 580nm was purchased from NN Crystal (Fayetteville, AR). CdSe/CdS quantum rods, 590nm peak emission was purchased from Strem (Newburyport, MA). Dark quencher QXL 570 acids, SE was purchased from AnaSpec (Fremont, CA). MeTz-PEG24-amine, methoxy-PEG24-amine and methoxy-PEG8-amine were purchased from BroadPharm (San Diego, California). N-(3-Dimethylaminopropyl)-N'-ethylcarbodiimide hydrochloride (EDC) and N-Hydroxy succinimide (NHS) were purchased from Sigma-Aldrich (St. Louis, MO).

### *4.2.2 Modification of Dark Quencher and silica particle preparation*

1.28 moles of organic dark quencher were reacted with the equivalent amount of APTS in ethanol. The reaction time was 24 hours at room temperature. This step was skipped if no dark quenchers were used.

The reaction started with using 1.3 mL IGEPAL-CO520 surfactant within 10 mL of cyclohexane in a 20 mL glass vials. Sonicated for 1 min. Next, organic dyes or quantum dots were added, sonicated for 5 mins. 150 μL ammonium hydroxide was added and was sonicated for 1 min. Finally, 80 μL of TEOS was added and allowed to react for 24 hours at room temperature to produce silica particle shells. 4 μL of carboxyethylsilanetriol and 2 μL of 3-(Trihydroxysilyl) propyl methylphosphonate were added.

After 24 hours, synthesis was mix with 0.5 volume equivalents of methanol, followed with vortex. The mixture was centrifuged at 15000 rpm for 20 min. The supernatant was removed. The pellets were dissolve with 50% of ethanol by sonicating. The dissolved solution was transferred into an Amicon filter, followed by centrifuging. The particles were purified in 50% ethanol two times, followed with purified water one time. The particle samples stored at 4 °C.

### *4.2.3 Primary PEGylation of Silica Particles*

15 nM of particles were reacted with 100 μM of PEG24, including 20% MeTz-PEG24 and 80 % mPEG24, 300 μM of EDC and 90 μM of NHS. After 3

hours, the synthesis was purified by a 100kDa Amicon filter, followed by three times of wash with water. The particle samples were stored at 4 °C.

### *4.2.4 Backfilled PEGylation of Silica Particles*

15 nM of particles were reacted with 100 μM of mPEG8, 300 μM of EDC and 90 μM of NHS. After 3 hours, the synthesis was transferred into a 100K Amicon filter for purification. It was washed by water for three times. The particle samples were stored at 4 °C.

### *4.2.5 Techniques*

Many techniques were used to test the particle samples and the labeling cells. The analysis included dynamic light scattering (DLS) to determine probe size with a Malvern Zetasizer Nano DLS system, fluorometry with a Tecan Spark multimode microplate reader, absorbance with a Nanodrop, scanning electron microscopy (SEM) with a FEI Magellan 400 XHR system, transmission electron microscopy (TEM) with a JEOL-2100F, fluorescence confocal microscopy with a Leica TCS SP8, the phasor approach using a custom-built FLIM system (M1, 20 MHz) and software (SimFCS) developed by the Laboratory for Fluorescence Dynamics at the University of California, Irvine.

## 4.3 Results and Discussion

### *4.3.1 Size measurement of QD with Silica Shells*

CdSe/ZnS (CZ) quantum dots and CdSe/CdS (S) quantum rods with different amounts of Dark quencher QXL 570 within silica shells were synthesis. The particles were measured by DLS (Maverick, CA) and TEM (JEOL-2100F). The sizes were between 30-80 nm. Lowering the amounts of quantum dots resulted in the increase of particle size in the conditions without dark quencher being added for CZ particles, shown in figure 4.1. The size expansion is caused by solvent. The quantum dots were in toluene when added. Different amounts toluene changed the hydrophilicity of the emulsion system. Additionally, when the same amounts of quantum dots were added, particles with larger amounts of dark quenchers have larger sizes. Dark quenchers were modified with silanes before adding into the emulsion. Adding more dark quenchers means adding more silane at the same time, which makes the particles bigger. However, it doesn't happen to all the conditions.

TEM images showed that the quantum dots/rots, which was the darker areas, were encapsulated within silica shells, which was the grey areas. Interestingly, all the silica particles have quantum dots in them when 200 µl of CZ quantum dots were added. Some particles have no quantum dots when less amounts or quantum

dots were added. More empty silica particles existed when smaller amount of CZ was used. Similar phenomenon happened to S quantum rods as well.

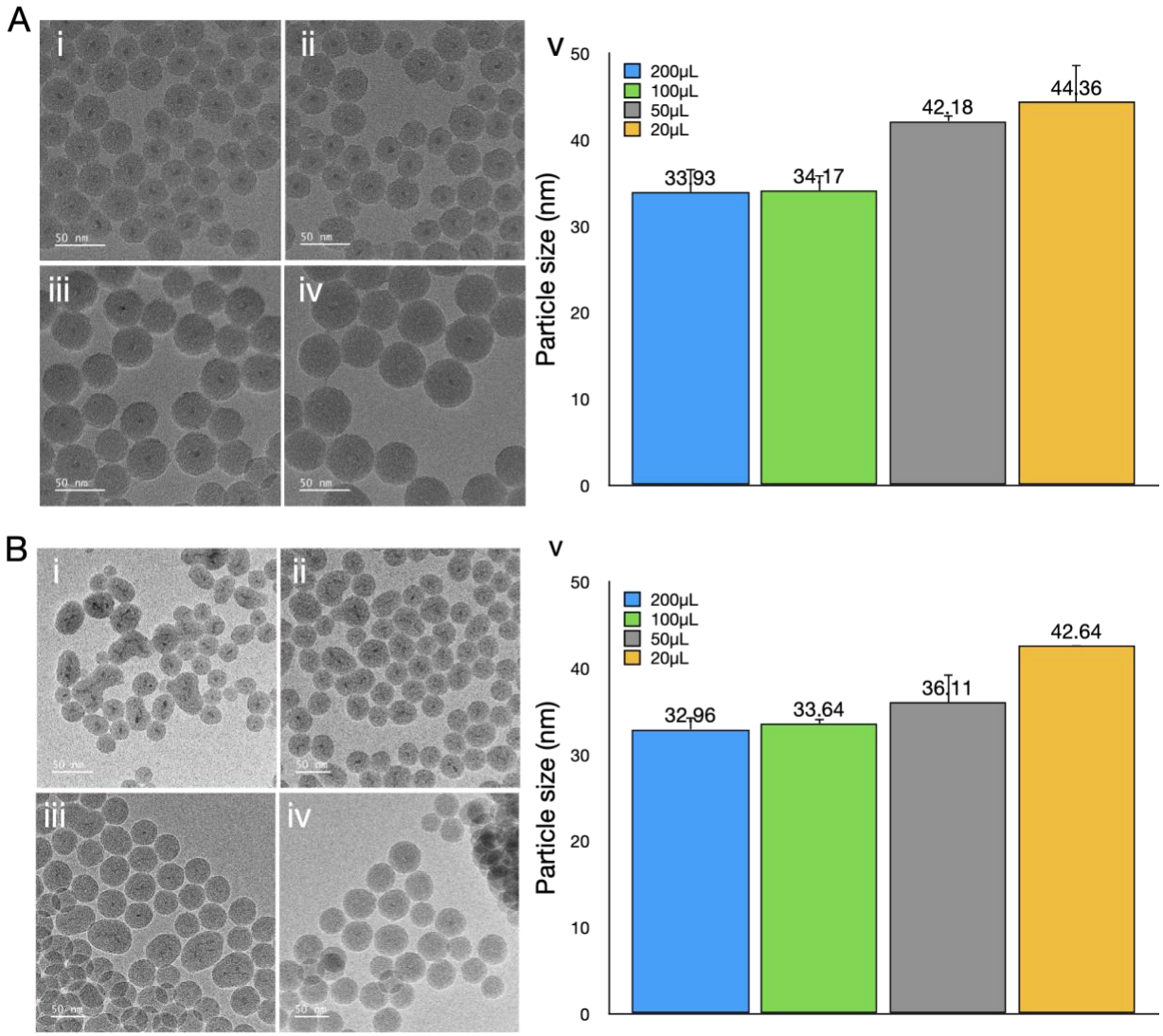



**Figure 4.2 Size analysis of QDs in silica shells.** (A) 200, 100, 50 and 20 μL of CdSe/ZnS quantum dots were added during synthesis. TEM images were collected (i-iv). And DLS results (v) shows that particle size increases with fewer quantum dots added. (B) 200, 100, 50 and 20 μL of CdSe/CdS quantum rods were added during synthesis. TEM images were collected (i-iv). And DLS results (v) shows that particle size increases with fewer quantum rods added. Scale bar is 50 nm.

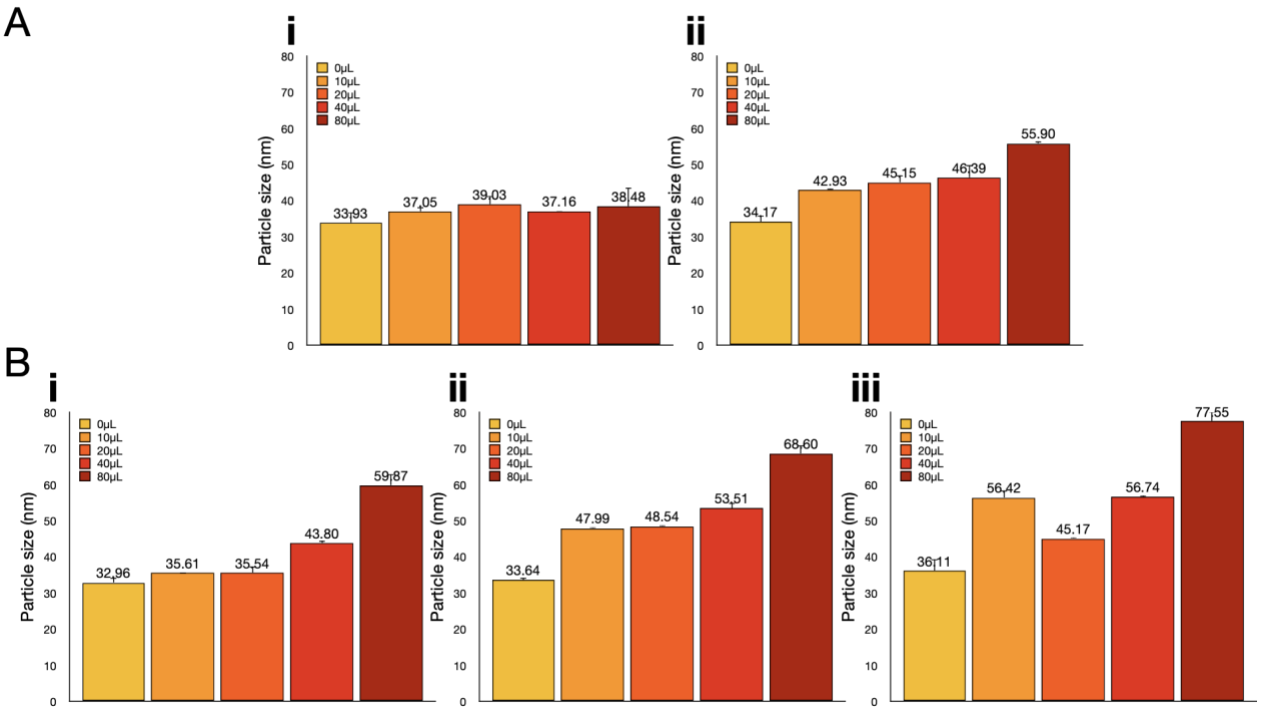



**Figure 4.4 DLS measurement of QDs with dark quencher in silica shells.** (A) CdSe/ZnS quantum dots with dark quencher: 200 and 100 µL (i-ii) of CdSe/ZnS quantum dots were added during synthesis. 0, 10, 20, 40 and 80 µL of dark quencher were used. (B) CdSe/CdS quantum rods with dark quencher: 200, 100 and 50µL (i-iii) of CdSe/CdS quantum rods were added during synthesis. 0, 10, 20, 40 and 80 µL of dark quencher were used.

### *4.3.2 Emission measurement of QD with Silica Shells*

Emission spectra of quantum dots/rods were measured by the Spark multimode microplate reader (Tecan, Switzerland) and emission maxima was analyzed. The particle concentrations were the same when the spectra were measured, so that the intensities of different conditions could be compared. We first measured 200, 100, 50, and 20 µL of CZ quantum dots and S quantum rods with silica shells. All the CZ particles showed peaks at the same wavelength. And

larger amounts of CZ quantum dots had stronger signal. However, S200 had a lower intensity than S100 due to self-quenching, which usually causes intensity declines. And the red shift in the emission spectra with increase of the amounts of S quantum rods further proved the quenching effect. After that, the emission of quantum dots/rods with different amounts of darker quencher were measured. 0, 10, 20, 40, 80 µL of dark quenchers were added combined with 200, 100 µL of CZ and 200, 100 and 50 µL of S quantum rods, respectively. The emission maxima decreased when larger amounts of darker quencher were added, because the energy emitted by the quantum dots were absorbed by dark quencher and dissipated as heat.

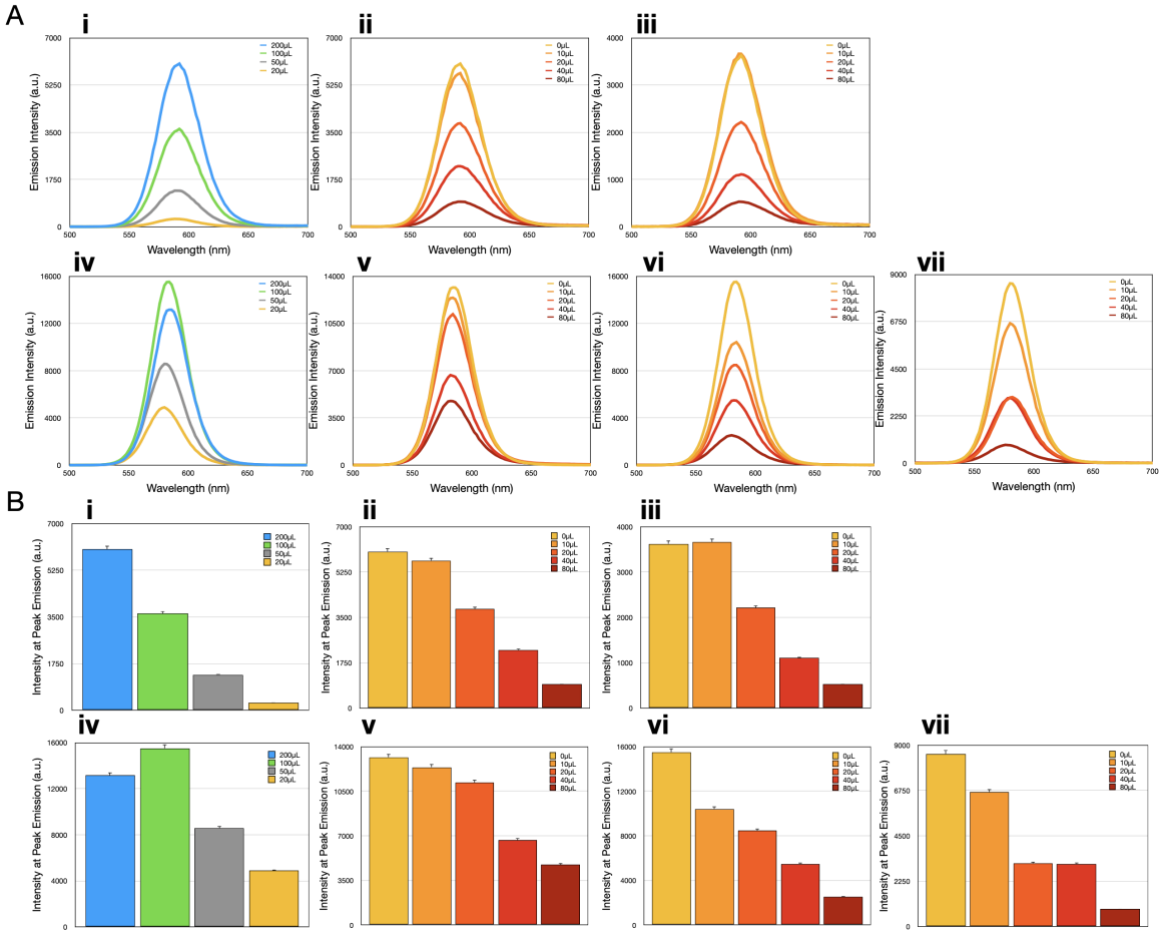



**Figure 4.6 Emission analysis of QDs in silica shells.** Emission spectra (A) and Emission Maxima (B) of 200, 100, 50 and 20 µL of CZ (i); 200, 100, 50 and 20 µL of S (iv); 200 µL of CZ with dark quencher(ii); 100 µL of CZ with dark quencher (iii); 200 µL of S with dark quencher (v); 100 µL of S with dark quencher (vi); and 50 µL of S with dark quencher (vii). 0, 10, 20, 40, 80 µL of dark quencher were added.

### *4.3.3 Lifetime measurement of QD with Silica Shells*

The lifetimes of quantum dots and quantum dot/dark quencher QXL 570 mixtures silica nanoprobes were measured by a fluorescence lifetime microscope (M1,

LFD). They were all in water when the lifetimes were acquired. I first measured the silica particles with pure quantum dots and later the quantum dots/darker quencher particles. The amounts of quantum dots used had little effect on the lifetime, but the lifetime increased with more quantum dots added due to passivation of quantum dot surface, prevented non-radiative recombination. The amount of dark quencher used played a much more important role in manipulating the lifetimes. The lifetimes were elongated when more dark quenchers were added. The lifetime phasors of different conditions were displayed in figure 4.4 A. The phasor of all conditions combined, as well as the phasor of selected conditions were shown in figure 4.4 B. The lifetimes of different conditions spread out in the combined phasor, which demonstrated the feasibility of using these particles for multiplexing. Many factors were considered during the selection of nano probes. The most important factor was lifetime similarity. The lifetimes were shown as different clusters in a phasor plot. We wanted to have the lifetime spread out as possible and keep enough space between different lifetime clusters. If two or more lifetime clusters were too close or even overlapped, factors like emission intensity and particle sizes were taken into consideration. Probes with too high or too low intensities were avoided. Similarly, probes with large sizes were not preferable.

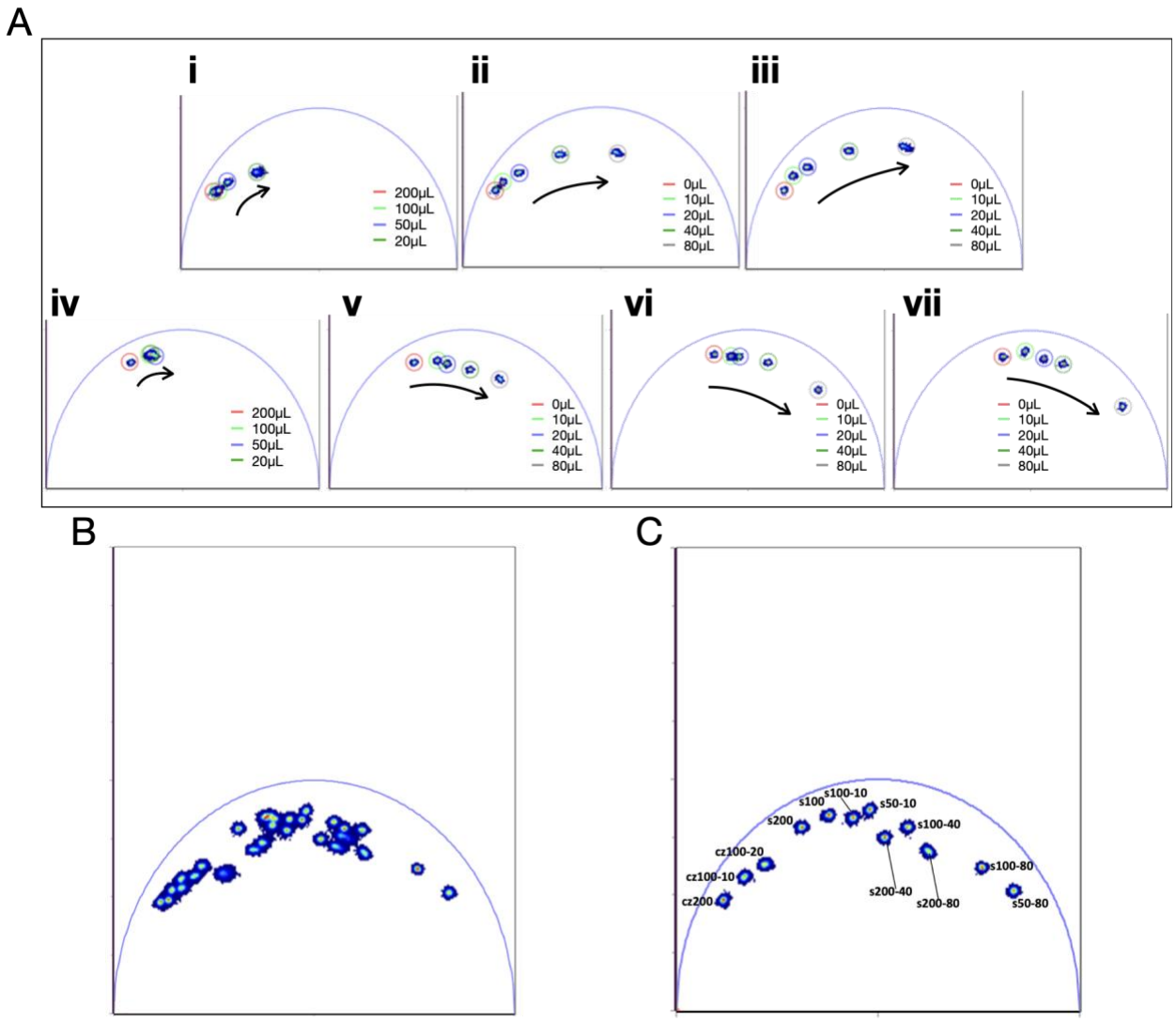



**Figure 4.8 Lifetime analysis of QDs in silica shells.** (A) Lifetime phasors, (B) the combined phasor and (C) the refined phasor of 200, 100, 50 and 20 µL of CZ (i); 200 µL of CZ with dark quencher(ii); 100 µL of CZ with dark quencher (iii); 200, 100, 50 and 20 µL of S (iv); 200 µL of S with dark quencher (v); 100 µL of S with dark quencher (vi); and 50 µL of S with dark quencher (vii). 0, 10, 20, 40, 80 µL of dark quencher were added.

## 4.4 Conclusion

In summary, it was shown that the lifetime library was made by utilizing dynamic quenching effect. The silica particles were prepared with different amounts of CZ and S quantum dots/rods. The particles were imaged by TEM to show that adding fewer quantum dots/rods results in some empty silica particles. DLS results showed that adding more quantum dots made the silica particles larger. Emission measurement demonstrated the dynamic quenching effect. The bright quantum dots mixed with dark quencher and the lifetime were shortened by adding more dark quenchers. Emitted energy was transferred to dark quencher molecule and released as energy. In this case, lifetimes were shortened, and emission signals were weakened. After carefully considering factors like lifetime difference, size and brightness, the quantum dot silica particle library containing 12 nanoprobes was built. The quantum dot library was able to be used for building panels for multiplexing.

# CHAPTER 5 Measuring Lifetime of Organic Dyes with Silica Shells using FLIM

## 5.1 Introduction

It was demonstrated that the silica particles could be used as probes for cancer cell receptor detection in chapter 3. It was shown in chapter 4 that fluorescent lifetimes were adjusted by using dark quencher. And a lifetime library of quantum dots and dark quencher was presented in chapter 4.

In this chapter, I will present a lifetime library using organic dyes. First, I prepared nanoprobes with seven types of organic dyes. The lifetime was changed when different amounts of dyes were used due to self-quenching effect. Energy was absorbed by the neighboring dye molecule and was lost during the process. Secondly, the size, emission and lifetimes of different conditions were measured. Lastly, a lifetime library of organic dye silica particles was built based on factors like lifetime, particle size and emission intensity.

## 5.2 Materials and Methods

### *5.2.1 Materials*

Cyclohexane, (3-Aminopropyl) triethoxysilane (APTS), IGEPAL-CO520 surfactant, Tetraethylorthosilicate (TEOS), Ammonium hydroxide (30% in water),

3-(Trihydroxysilyl) propyl methylphosphonate (TPMP) were purchased from Sigma-Aldrich (St. Louis, MO). Carboxyethylsilanetriol (CEST) was purchased from Gelest (Morrisville, PA). Methanol and Ethanol purchased from Sigma-Aldrich (St. Louis, MO). Amicon Ultra Centrifugal Filter (100kDa) was purchased Millipore Sigma. BODIPY™ TMR-X NHS Ester, NHS-Rhodamine, Alexa Fluor™ 555 NHS Ester, DyLight™ 550 NHS-Ester were purchased from Fisher Scientific (Waltham, MA). ATTO Rho3B NHS-ester was purchased from ATTO-TEC GmbH (Siegen, Germany). FSD FluorTM 555 NHS-ester was purchased from Bioacts (Incheon, South Korea). MeTz-PEG24-amine, m-PEG24-amine and m-PEG8-amine were purchased from BroadPharm (San Diego, California). N-(3-Dimethylaminopropyl)-N'-ethylcarbodiimide hydrochloride (EDC) and N-Hydroxy succinimide (NHS) were purchased from Sigma-Aldrich (St. Louis, MO).

### *5.2.2 Modification of Organic dyes and Silica Particle Preparation*

1.28 moles of organic dyes were reacted with the equivalent amount of APTS in 500 μL of ethanol. The reaction time was 24 hours at room temperature.

The reaction started with using 1.3 mL IGEPAL-CO520 surfactant within 10 mL of cyclohexane in a 20 mL glass vials. Sonicated for 1 min. Next, organic dyes were added, sonicated for 5 mins. 150 μL ammonium hydroxide was added, followed by sonicating for 1 min. Finally, 80 μL of TEOS was added and allowed

to react for 24 hours at room temperature to produce silica particle shells. 4 μL of carboxyethylsilanetriol and 2 μL of 3-(Trihydroxysilyl) propyl methylphosphonate were added.

After 24 hours, synthesis was mix with 0.5 volume equivalents of methanol. The mixture was centrifuged at 15000 rpm for 20 min. The supernatant was removed. The pellets were dissolved with 50% of ethanol by sonicating. The dissolved solution was transferred into an Amicon filter, followed by centrifuging. The particles were purified in 50% ethanol two times, and water one time. The particle samples stored at 4 °C.

### *5.2.3 Primary PEGylation of Silica Particles*

15 nM of particles were reacted with 100 μM of PEG24, including MeTz-PEG24 and mPEG24 reacted, 300 μM of EDC and 90 μM of NHS. After 3 hours, the synthesis was transferred into a 100K Amicon filter for purification, followed by three times of wash with water. The particle samples were stored at 4 °C.

### *5.2.4 Backfilled PEGylation of Silica Particles*

15 nM of particles were reacted with 100 μM of mPEG8, 300 μM of EDC and 90 μM of NHS. After 3 hours, the synthesis was transferred into a 100kDa Amicon filter for purification. It was washed by water for three times. The particle

samples were measured by absorption measurement and calibration curve, and stored at 4 °C.

### *5.2.5 Techniques*

Many techniques were used to test the particle samples and the labeling cells. The analysis included dynamic light scattering (DLS) to determine probe size with a Malvern Zetasizer Nano DLS system, fluorometry with a Tecan Spark multimode microplate reader, absorbance with a Nanodrop, scanning electron microscopy (SEM) with a FEI Magellan 400 XHR system, transmission electron microscopy (TEM) with a JEOL-2100F, fluorescence confocal microscopy with a Leica TCS SP8, the phasor approach using a custom-built FLIM system (Alba, 80 MHz) and software (SimFCS) developed by the Laboratory for Fluorescence Dynamics at the University of California, Irvine.

## 5.3 Results and Discussion

### *5.3.1 Size measurement of Dye with Silica Shells*

The sizes of seven types of fluorescent dyes with silica shells were measured. 1, 3, 10, 20, 40, 80 and 120 µL of each dye were used for silica particle synthesis. Briefly, organic dyes were modified by APTS. After 24 hours, silanized dyes were wrapped into silica by addition of TEOS. After the silica particles were

washed, the supernatants were measured by DLS. The size of particles increased with the amounts of dye increased. When 80 and 120 µL of dyes were added, particles aggregated and enlarged the aqueous size.

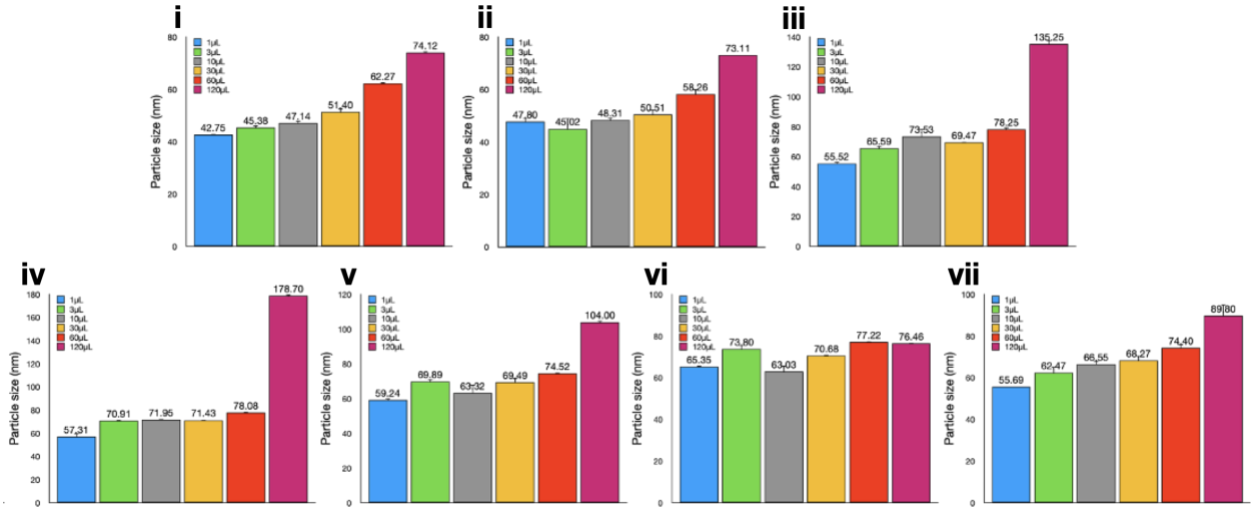



**Figure 5.2 DLS measurement of organic dyes in silica shells.** Size of AlexaFluor555 (i), BodipyTMR (ii), Rhodamine (iii), FSD555 (iv), ATTO Rho3B (v), DyLight550 (vi) and KU530 (vii) were added for particle synthesis. 1, 3, 10, 30, 60, 120 µL of dyes were used.

### *5.3.2 Emission measurement of Dye with Silica Shells*

The emission spectra measured by Spark multimode microplate reader and intensity maxima were presented in figure 5.2. The wavelength at peak emission showed a red shift with the increase of dyes amounts, which demonstrated that self-quenching happened. The mechanism of quenching is complex and mostly of the time several factors have a joint effect. The absence of shift in absorption spectra indicated that there was no change in ground state when the dye molecules

were excited. High concentration played an important role. The dye molecules had small stokes shift, which meant their absorption and emission spectra were close. The dyes were encapsulated inside silica shells, which led to high local concentrations. Thus, dye molecules were close to each other (within a few tens of nanometers). Light was prevented from emitting due to re-absorption, in which energy was dissipated. And the decrease of intensity in high concentration further proved that.

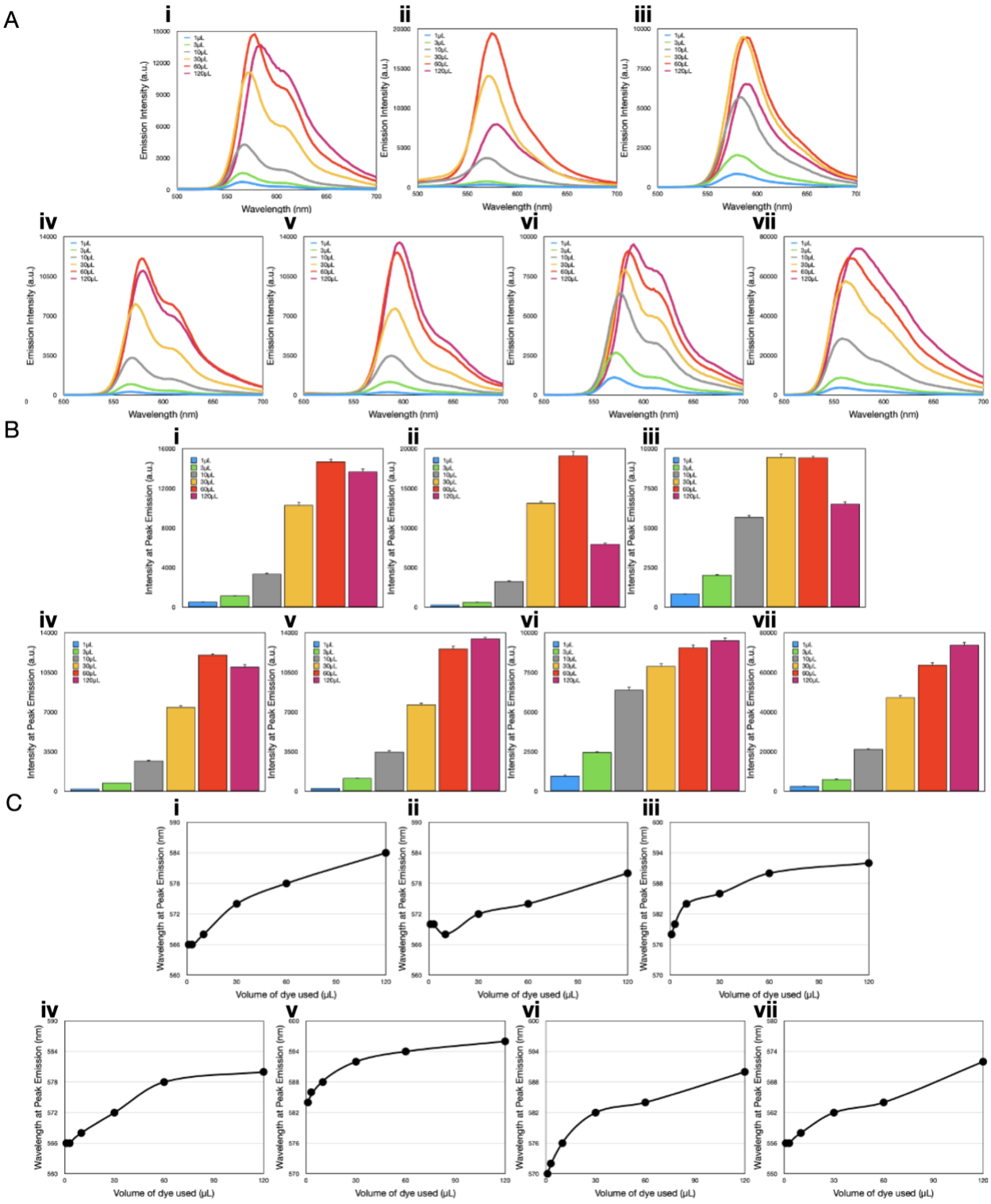



**Figure 5.4 Emission analysis of organic dyes in silica shells.** Emission spectra (A), Emission Maxima (B), and red shift of wavelength at peak (C) of

AlexaFluor555 (i), BodipyTMR (ii), Rhodamine (iii), FSD555 (iv), ATTO Rho3B (v), DyLight550 (vi) and KU530 (vii). 1, 3, 10, 30, 60, 120 μL of dyes were used.

### *5.3.3 Lifetime measurement of Dye with Silica Shells*

The lifetime of seven types of dye silica nano probes were measured by a 80 MHz fluorescent lifetime microscope at LFD, UC Irvine. Different amounts of fluorescent dyes were used for particle synthesis. The lifetime of each dye and a combined phasor were presented. The phasors showed that the lifetime was shortened with increasing dye amounts due to self-quenching. Fluorescence happens when a dye molecule moves from an exited state to the ground state. Energy is released. And the lifetime is defined as the time it takes for the process to happen. In this case, the emission signal was transferred to the neighboring molecules through non-radiative. This led to a decrease in lifetime because energy was dissipated without emitting photons. The lifetime spans whole range of the combined phasor, which demonstrated that the lifetime was able to be manipulated by trapping different amounts of dyes in silica nano particles. A refined lifetime library was built based on factors like lifetime distance, size, and intensity. And this lifetime library could be used for multiplexing.

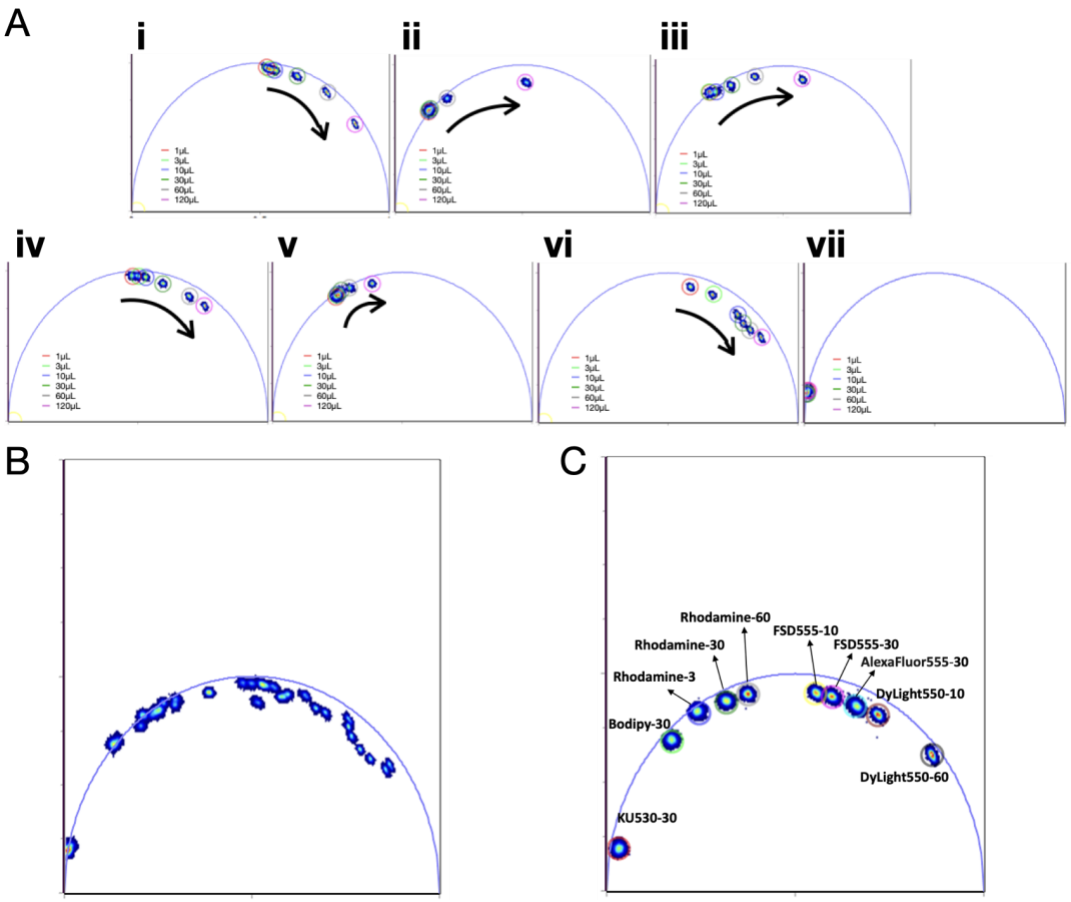



**Figure 5.6 Lifetime measurement of organic dyes in silica shells.** (A) Lifetime phasors of seven organic dye silica particle solutions: AlexaFluor555 (i), BodipyTMR (ii), Rhodamine (iii), FSD555 (iv), ATTO Rho3B (v), DyLight550 (vi) and KU530 (vii). 1, 3, 10, 30, 60, 120 µL of dyes were used. (B) Lifetime phasor of all the conditions. (C) Lifetime library of dye particle in silia shells. The lifetime conditions were selected by lifetime, emission intensity and particle size.

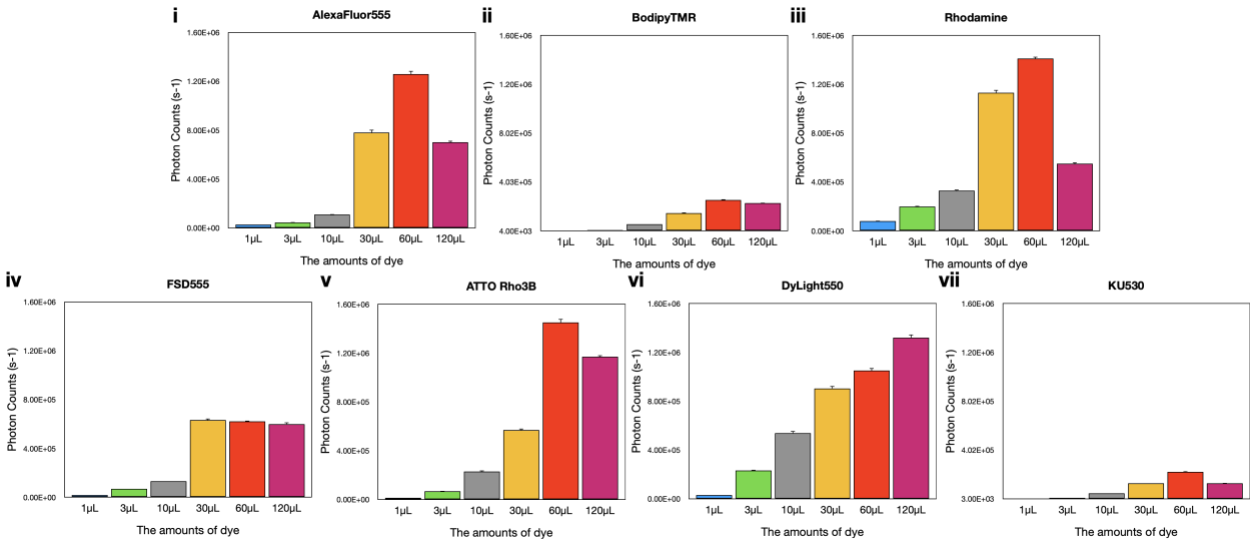



**Figure 5.8 Photon counts of organic dye silica particles in solution.** Photon counts of seven organic dye silica particle solutions: AlexaFluor555 (i), BodipyTMR (ii), Rhodamine (iii), FSD555 (iv), ATTO Rho3B (v), DyLight550 (vi) and KU530 (vii). 1, 3, 10, 30, 60, 120 μL of dyes were used. The photon counts were collected when the lifetimes were measured.

## 5.4 Conclusion

In conclusion, a fluorescent lifetime library was built by utilizing self-quenching effect. Seven organic dyes were used for preparing the silica particles. Different amounts of dyes were used. The lifetime was reduced with the amount of dye increasing. The emission intensities reduction and the shift of emission max proved the existence of self-quenching effect. All the lifetime conditions were summarized and put into a lifetime phasor. After considering the particles size, emission signals and lifetime, a more refined version of lifetime was presented. Ten nanoprobes were presented in the final version of the phasor plot.

# CHAPTER 6 Application of Silica Probes on Breast Cancer Cells using FLIM

## 6.1 Introduction

It was demonstrated that the silica probe modified with PEGs was able to conjugate to breast cancer cells via specific bindings. And later lifetime libraries were presented to demonstrate that lifetime could be adjusted by using different fluorophore mixtures. In this chapter, I will present a lifetime library using both quantum dots/dark quencher and organic dyes. Then a tumor panel was built and validated with the silica probes in cells.

First, a silica shell stability test was conducted to exam the protection effect of silica shells on organic dyes within. Next, I prepared nanoprobes of 11 conditions. I validated the lifetimes of each probe both on cells and solution. SKBR3 cells were stained with each of the probes via HER. The final version of lifetime library on cell consisting of 8 was presented. Lastly, I designed my tumor panel with four adhesive cell lines, by selecting probes from the final version of cell lifetime library.

## 6.2 Materials and Methods

### *6.2.1 Materials*

Cyclohexane, (3-Aminopropyl) triethoxysilane (APTS), IGEPAL-CO520 surfactant, Tetraethylorthosilicate (TEOS), Ammonium hydroxide (30% in water), 3-(Trihydroxysilyl) propyl methylphosphonate (TPMP) were purchased from Sigma-Aldrich (St. Louis, MO). Carboxyethylsilanetriol (CEST) was purchased from Gelest (Morrisville, PA). Methanol and Ethanol purchased from Sigma-Aldrich (St. Louis, MO). Amicon Ultra Centrifugal Filter (100kDa) was purchased Millipore Sigma. CdSe/ZnS quantum dots (CZ) 580nm was purchased from NN Crystal (Fayetteville, AR). BODIPY™ TMR-X NHS Ester, NHS-Rhodamine, Alexa Fluor™ 555 NHS Ester, DyLight™ 550 NHS-Ester were purchased from Fisher Scientific (Waltham, MA). FSD FluorTM 555 NHS-ester was purchased from Bioacts (Incheon, South Korea). MeTz-PEG24-amine, m-PEG24-amine and m-PEG8-amine were purchased from BroadPharm (San Diego, California). N-(3-Dimethylaminopropyl)-N'-ethylcarbodiimide hydrochloride (EDC) and N-Hydroxy succinimide (NHS) were purchased from Sigma-Aldrich (St. Louis, MO).

### *6.2.2 Modification of Organic dyes*

1.28 moles of organic dyes were reacted with the equivalent amount of APTS in 500 μL of ethanol. The reaction time was 24 hours at room temperature. This step was skipped if no organic dyes or dark quenchers were used.

The reaction starts with using 1.3 mL IGEPAL-CO520 surfactant within 10 mL of cyclohexane in a 20 mL glass vials. Sonicated for 1 min. Next, organic dyes or quantum dots were added, sonicated for 5 mins. 150 μL ammonium hydroxide was added, followed by sonicating for 1 min. Finally, 80 μL of TEOS was added and allowed to react for 24 hours at room temperature to produce silica particle shells. 4 μL of carboxyethylsilanetriol and 2 μL of 3-(Trihydroxysilyl) propyl methylphosphonate were added.

After 24 hours, synthesis was mix with 0.5 volume equivalents of methanol. The mixture was centrifuged at 15000 rpm for 20 min. The supernatant was removed. The pellets were dissolved with 50% of ethanol by sonicating. The dissolved solution was transferred into an Amicon filter, followed by centrifuging. The particles were purified in 50% ethanol two times, and water one time. The particle samples stored at 4 °C.

### *6.2.3 Primary PEGylation of Silica Particles*

15 nM of particles were reacted with 100 μM of PEG24, including MeTz-PEG24 and mPEG24 reacted, 300 μM of EDC and 90 μM of NHS. After 3 hours, the synthesis was transferred into a 100K Amicon filter for purification, followed by three times of wash with water. The particle samples were stored at 4 °C.

### *6.2.4 Backfilled PEGylation of Silica Particles*

15 nM of particles were reacted with 100 μM of mPEG8, 300 μM of EDC and 90 μM of NHS. After 3 hours, the synthesis was transferred into a 100kDa Amicon filter for purification. It was washed by water for three times. The particle samples were measured by absorption measurement and calibration curve, and stored at 4 °C.

### *6.2.5 Antibody Modification*

200 μg of HER2 antibody was reacted with 30 mole equivalents of NHS-TCO in PBS+ with 10% total volume of DMF and sodium bicarbonate (0.1M, pH=8.4) at room temperature for 3 hours. Modified antibody was purified by 40K ZebaTM Spin Desalting Column. The concentration of the purified sample was measured by absorption measurements using NanoDrop.

### *6.2.6 Cell Culture and Cell labeling*

SKBR3 cell line was maintained in McCoy's 5A 1x base media, supplemented with 10% FBS, 1% Pen/Strep and 1% L-glutamine. Cells were incubated at 37 ºC and supplied with 5% CO2.

Cells were plated in 8-well microscope chambers 2-3 days prior to imaging and made sure the cell confluency reached 75~80% when used.

The cells were washed with PBS+ one time to remove the media. For one-step staining, cells were directly stained by immunoconjugates and incubated for

30 mins. For two-step staining, cells were first stained by TCO-modified HER2 antibodies at 10 μg/mL for 30 mins, followed by adding Tz-modified silica particles for 20 mins. The incubation process was conducted at room temperature, and after each incubation step, cells were washed with PBS+ to remove excess antibodies. 200 μL of fixing buffer (1:1) was added into each well. After 20 mins of incubation, fixing buffer was removed. The cells were washed with PBS once and PBS+ twice. Finally, 200 μL of PBS+ was added into each cell well for imaging.

Stained cells were imaged by a fluorescence lifetime microscope (Alba, Laboratory for Fluorescence Dynamics at UCI). Samples were excited at 555 nm, and the emission window is 565-605 nm.

### *6.2.7 Techniques*

Many techniques were used to test the particle samples and the labeling cells. The analysis included dynamic light scattering (DLS) to determine probe size with a Malvern Zetasizer Nano DLS system, fluorometry with a Tecan Spark multimode microplate reader, absorbance with a Nanodrop, the phasor approach using a custom-built FLIM system (Alba, 80 MHz) and software (SimFCS) developed by the Laboratory for Fluorescence Dynamics at the University of California, Irvine.

## 6.3 Results and Discussion

### *6.3.1 Stability Test of Silica Shells*

I tested the protective effect of silica shells by exposing dyes with and without silica shells to bleach. The strong oxidizer hydrochloride damaged dye molecules and caused photon bleaching. The fluorescence signal photon counts were measured by 80 MHz fluorescence lifetime microscope at LFD. The dyes and dye particles treated with water were used as controls. The fluorescence signals under different bleach concentrations were normalized and presented in figure 6.1. In all seven dye conditions, either free dyes or silica particles, the fluorescence signal dropped when bleach concentration increased. More importantly, the fluorescence of silica particles lost more slowly than the signal of free dyes with bleach concentration increasing, which meant the dyes protected by silica shells were more resistant with bleach. It demonstrated that the silica shells served as a protective shield. The silica shell enhanced the stability of dyes and widened the range of their applications, especially in biomedical fields.

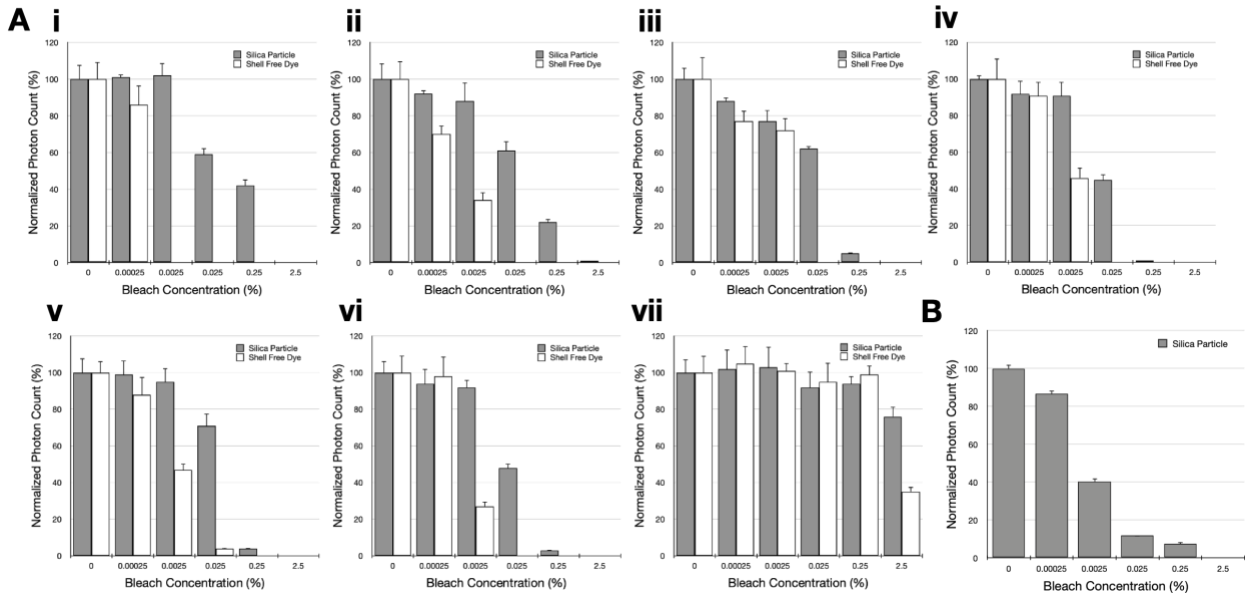



**Figure 6.2 Protection effect of silica shells.** (A) Dye particles and free dyes were treated by 0.00025, 0.0025, 0.025, 0.25 and 2.5% of Clorox bleach. The control groups were treated by water. 60 µL of AlexaFluor555 (i), BodipyTMR (ii), Rhodamine (iii), FSD555 (iv), ATTO Rho3B (v), DyLight550 (vi) and KU530 (vii) were used for particle synthesis. (B) 200 µL of CZ particles was used for synthesis, and the particles were treated by 0.00025, 0.0025, 0.025, 0.25 and 2.5% of Clorox bleach.

### *6.3.2 Lifetime measurement of silica probes on cells*

We were trying to utilize the lifetime library to differentiate breast cancer cell types using the 80MHz fluorescence lifetime microscope. The probes were excited at 555 nm. The lifetimes of quantum dot probes were overlapping on the far-left side at a 80 MHz phasor, due to their long lifetimes. And KU dye had long lifetime, but its signal was weak at 555 nm excitation wavelength. Therefore, CZ 200 probes was used to replace KU. Each of the proves was measured on cells and

in solution. The test was conducted on skbr3 cells via HER2. The lifetime library on cells for tumor panel was built.

The lifetimes of nano probes on cells were more inner than those in solutions, shown from figure 6.2. It was the results of auto fluorescence due to the complex cell environment.

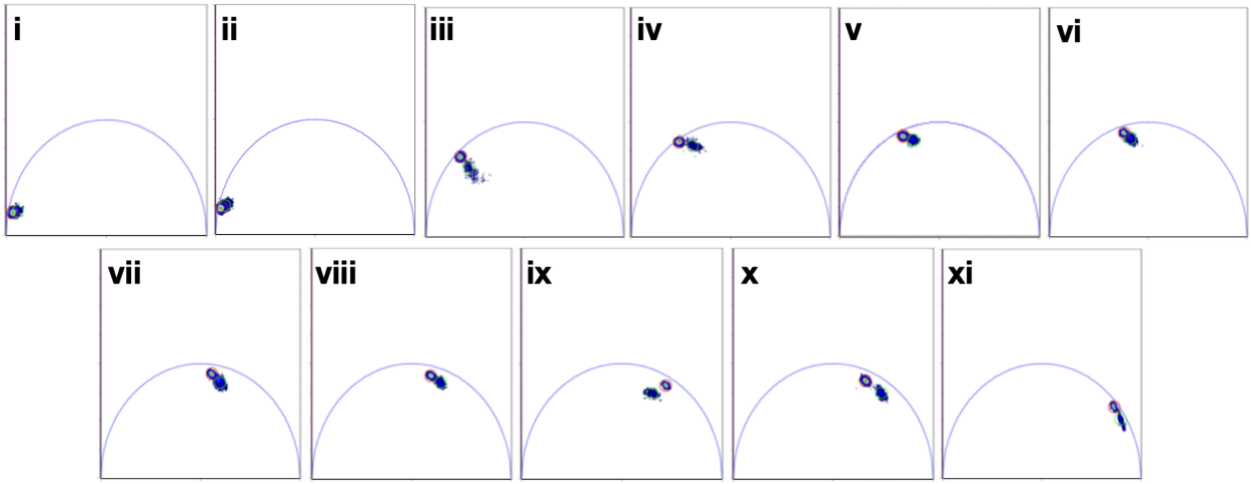



**Figure 6.4 Lifetime comparison of probes in solution and on cells.** Lifetime of eleven nanoprobes were measured in solution (red circles) and on cells (green circles). 200 µL CZ QD (i), 30 µL KU530 (ii), 30 µL BodipyTMR (iiii), 3 µL of Rhodamine (iv), 30 µL Rhodamine (v), 60 µL Rhodamine (vi), 10 µL FSD555 (vii), 30 µL FSD555 (viii), 30 µL AlexaFluor555 (ix), 10 µL DyLight550 (x) and 60 µL DyLight550 (xi) were used for particle preparation.

The confocal images of each probe were collected. The surface of cells was stained by nanoprobes. Due to the variety of nanoprobe brightness, the staining signals varied among different probes. And the lifetime information was measured and summarized in a combine phasor.

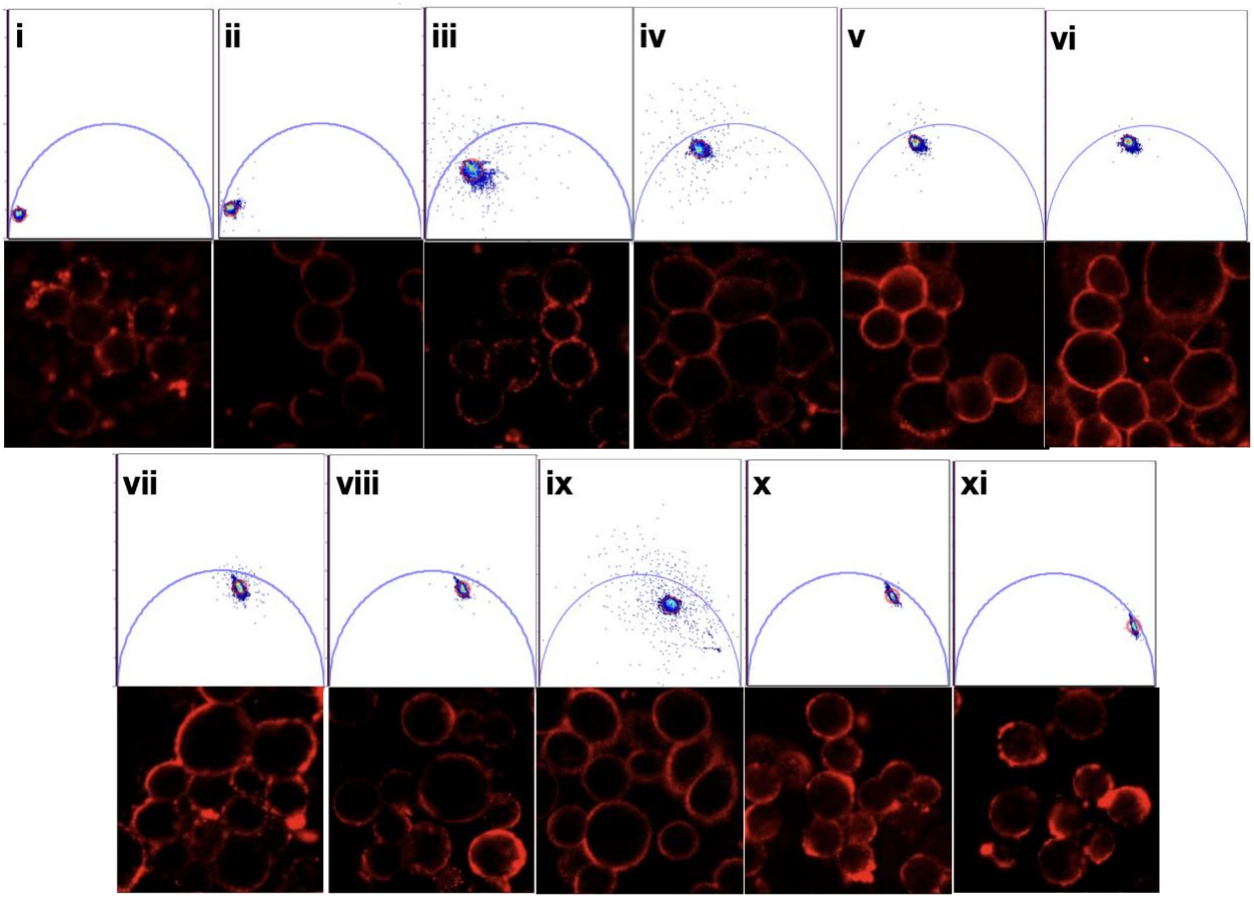



**Figure 6.6 Lifetime library of eleven probes on cells.** Confocal images and lifetimes of 200 µL CZ QD (i), 30 µL KU530 (ii), 30 µL BodipyTMR (iiii), 3 µL of Rhodamine (iv), 30 µL Rhodamine (v), 60 µL Rhodamine (vi), 10 µL FSD555 (vii), 30 µL FSD555 (viii), 30 µL AlexaFluor555 (ix), 10 µL DyLight550 (x) and 60 µL DyLight550 (xi) silica nanoprobes.

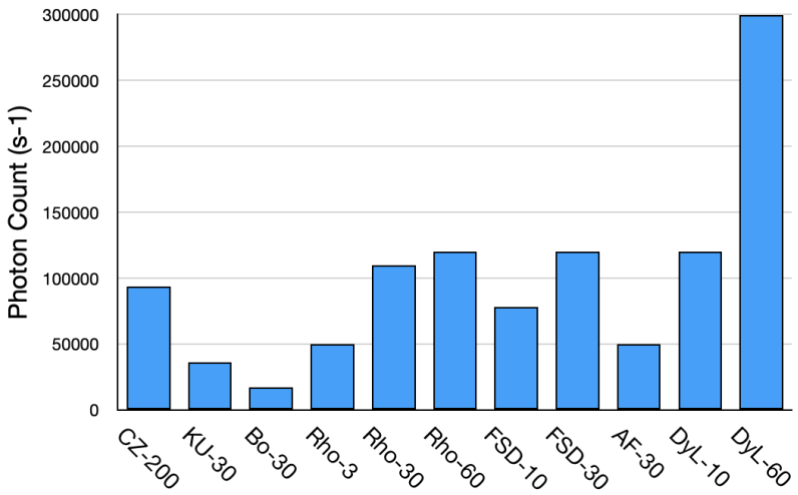



**Figure 6.8 Photon counts of eleven probe candidates on cells.** Photon counts of eleven silica nanoprobes candidates on cells.The photon counts were collected when the lifetimes were measured.

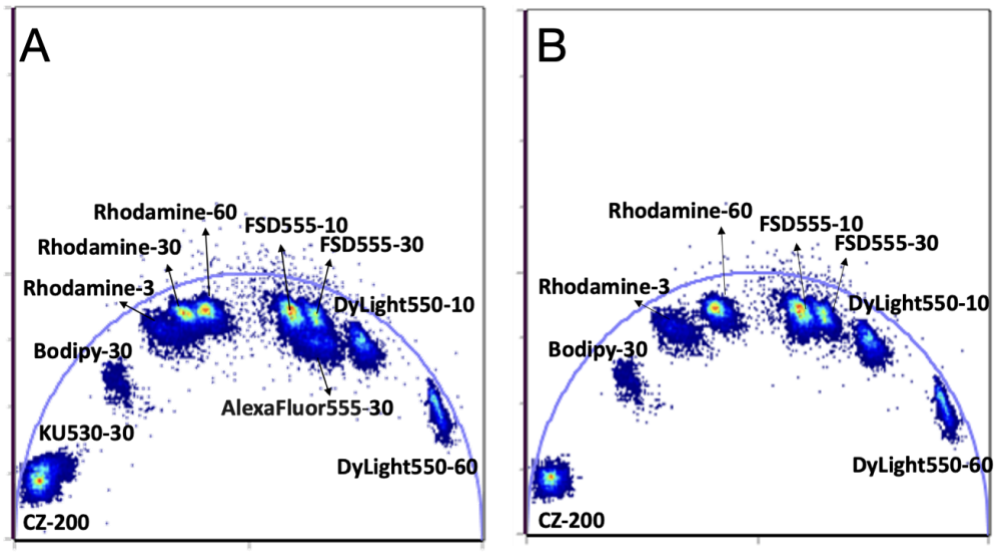



**Figure 6.10 Building lifetime library of silica probes on cells.** (A) Lifetime of all the silica nanoprobe candidates on cells. (B) Lifetime library of silica nanoprobes on cells. The lifetime conditions were selected by lifetime, emission intensity and particle size.

### *6.3.3 Design of tumor panel*

For the tumor panel, SKBR3, MDAMB231, MCF7 and BT474 were considered. The receptors of each cell lines were shown below in table 5.1. To cover all biomarkers over four cell types, six nano probes were used in corresponding to six biomarkers. The design was shown in figure 5.6.

**Table 6.1 Biomarker expression of four breast cancer cell lines. '+' means a biomarker is expressed.**

| | EpCAM | HER2 | TfR | Ecad | CD44 | PD-L1 |
|---|---|---|---|---|---|---|
| **SKBR3** | + | + | + | | | + |
| **MCF7** | + | | + | + | + | + |
| **MDA-MB-231** | | | + | | + | + |
| **BT474** | + | + | + | + | | |

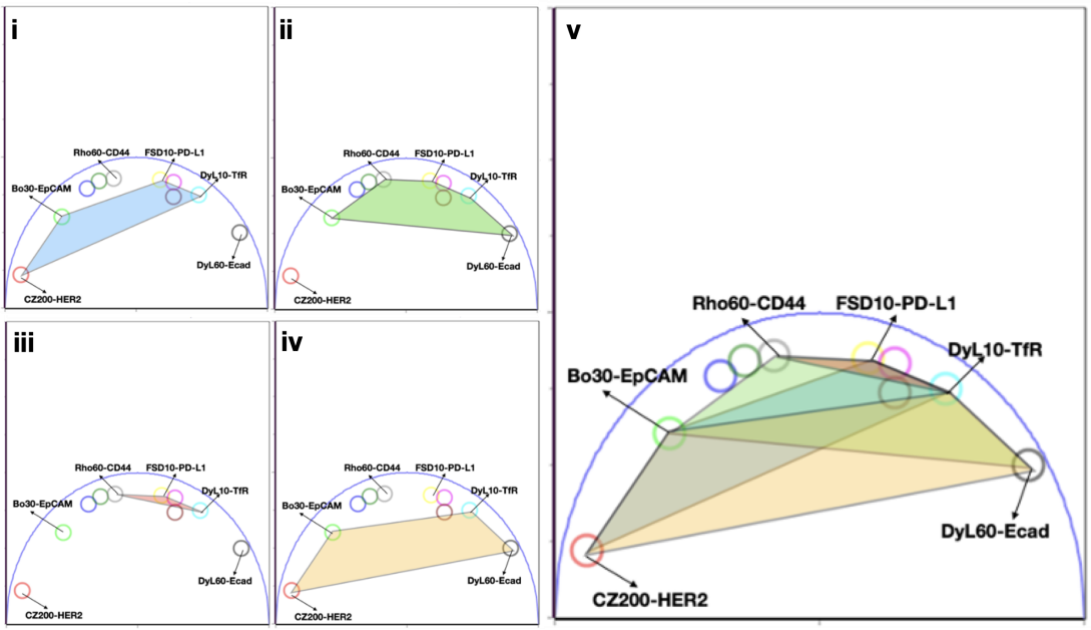


**Figure 6.6 Tumor panel design.** The multiplexing phasor for SKBR2 (i), MCF7 (ii), MDAMB231 (iii), BT474 (iv), four combined (v). The multiplexing lifetime of each cell line would be shown in the color area. (i-iv)

## 6.4 Conclusion

In conclusion, it was demonstrated that lifetime libraries could be used as cancer cell detection.

First, silica shells were able to isolate fluorescent species inside the particles and protect them from photo bleaching. Silica shells not only served as a carrier for lifetime adjustment, but also provided protection. However, the protection has a limit. The silica shells were penetrated when the bleach concentration is high.

What's more, a tumor panel was built using both quantum dots and organic dyes. The library for the panel was designed by factors including lifetime, particle size, and brightness. Ku dyes had long lifetime but were pretty dim at 555 nm wavelength. CZ quantum dots had long lifetime and showed in the left side of a 80 MHz phaser as well, but were brighter than KU. CZ was chosen. And other probes were chosen so that the lifetimes of probes were far enough to prevent overlapping. And the lifetime of all probes in tumor panel was validated. A final version of cell lifetime library with 8 conditions were used to design breast cancer panels over four different adhesive cell lines. It was shown that tumor panel could be used for detection and differentiating different cancer cell lines.

# CHAPTER 7 Conclusions and Future Directions

In conclusion, the fluorescence lifetime library based on silica nano particles was built and it was demonstrated that the library applied for breast cancer detection. To begin with, silica nanoprobes were prepared and validated on SKBR3 breast cancer cells. I synthesized silica particles via reverse micro emulsion. CZ quantum dots were used as an example. The particles were modified with both primary Methyl tetrazine PEG24 and backfilled PEG8. DLS and TEM results showed that the PEGylated silica particles were successful prepared. And the staining test proves that two-step and one-step staining with MeTz-PEG silica particles bound to HER2 on the surface of breast cancers. This silica particles could be used as fluorescence lifetime probes for cancer cell detection.

What's more, fluorescence lifetime libraries using PEGylated silica probes were built. Two methods were applied to change fluorescence lifetime. It happened because the fluorescent species were trapped within small silica particles. Dark quenchers were added to shorten the lifetime of bright quantum dots to build the first library. More dark quenchers were used, the shorter the lifetimes were. Emission was transferred to dark quencher and energy was released as heat. The second library replied on self-quenching. Larger amounts of fluorescent organic dyes resulted in shorter lifetimes. Emission was absorbed by neighboring dye molecules, and energy dissipation caused lifetime shortening. Quenching effects

happened because species were close enough, which was achieved by encapsulating them within nanoscale silica shells. Additionally, it was approved that silica shells could protect the fluorescent species from photo bleaching.

Lastly, it was proved that the fluorescence lifetime library could be used for a tumor panel. The tumor panel consisted of four cell lines: skbr3, MAD 231, MCF7 and BT474. In my design, six biomarkers were needed to distinguish the breast cancers cells. The lifetime of this library was measured at 555nm in 80 MHz, so many short lifetime organic dyes probes were chosen. Quantum dots generally have longer lifetimes and displayed their lifetime in the far-left side. Their lifetime overlapped with each other. And KU dyes have long lifetime but low emission signal. Therefore, one quantum condition was used to replace the KU dyes to make a new library for the tumor panel. Each of the probes were evaluated on breast cancer cells. In summary, it was proved that the silica probes and fluorescence lifetime libraries will be a powerful tool for detection cancer cells.

The idea of building fluorescence lifetime libraries with this innovative silica nano probes has promising future and will potentially lead to several further development. To begin with, applying nanoprobes to multiplex. Five to six probe-antibody conjugates are prepared and purified. Then they are added to cells at the same time. Because of the linear principle of phaser method, each of breast cells shows their unique pattern. With the algorithm that is developed by our lab, the

contribution of each probe/bio marker can be calculated. With this information, we can tell breast cancer cell types. What's more, the library can be applied to detect immune cells. Our lab has been working on lifetime multiplexing with fluorescent spices. With the biomarker information of different immune cells in hand, we can build a panel for immune cells. This silica probes will work well with the immune panel, which leads to greater clinical impact. Lastly, the silica probes will have potential applications in drug delivery. Silica particles have been used as drug carriers. Due to its biocompatibility and easily modification dynamics, the silica particles can carry drugs, either within the shells or by attached on the surface. Microenvironment of tumors are different from normal heathy cells, which can be a trigger for drug release. Additionally, it was demonstrated that the silica particles in the study attached to breast cancer cells via specific binding. The silica particles developed in this study can serve as not just a probe but also a drug carried for antibody therapy. However, more studies on absorption and excretion of the silica particles in vivo need to be conducted. The silica particles can combine fluorescence lifetime detection and antibody therapy, opening a new door for biomedical studies.

# REFERENCES


1. Wilkinson, L. and T. Gathani, *Understanding breast cancer as a global health concern.* The British journal of radiology, 2022. **95**(1130): p. 20211033.
2. Sung, H., et al., *Global cancer statistics 2020: GLOBOCAN estimates of incidence and mortality worldwide for 36 cancers in 185 countries.* CA: a cancer journal for clinicians, 2021. **71**(3): p. 209-249.
3. Qaseem, A., et al., *Screening for breast cancer in average-risk women: a guidance statement from the American College of Physicians.* Annals of internal medicine, 2019. **170**(8): p. 547-560.
4. Turner, K.M., et al., *Heterogeneity within molecular subtypes of breast cancer.* American Journal of Physiology-Cell Physiology, 2021. **321**(2): p. C343-C354.
5. Jin, X., et al., *Molecular classification of hormone receptor-positive HER2-negative breast cancer.* Nature Genetics, 2023. **55**(10): p. 1696-1708.
6. Swain, S.M., M. Shastry, and E. Hamilton, *Targeting HER2-positive breast cancer: advances and future directions.* Nature reviews Drug discovery, 2023. **22**(2): p. 101-126.
7. Thomas, A., et al., *Rare subtypes of triple negative breast cancer: current understanding and future directions.* NPJ Breast Cancer, 2023. **9**(1): p. 55.
8. Yin, L., et al., *Triple-negative breast cancer molecular subtyping and treatment progress.* Breast Cancer Research, 2020. **22**: p. 1-13.
9. Vidovic, D., et al., *ALDH1A3-regulated long non-coding RNA NRAD1 is a potential novel target for triple-negative breast tumors and cancer stem cells.* Cell Death & Differentiation, 2020. **27**(1): p. 363-378.
10. Tan, W.C.C., et al., *Overview of multiplex immunohistochemistry/immunofluorescence techniques in the era of cancer immunotherapy.* Cancer Communications, 2020. **40**(4): p. 135-153.
11. Selves, J., et al., *Immunohistochemistry for diagnosis of metastatic carcinomas of unknown primary site.* Cancers, 2018. **10**(4): p. 108.
12. Shidham, V.B. and L.J. Layfield, *Cell-blocks and immunohistochemistry.* Cytojournal, 2021. **18**.
13. Huang, Y.-K., et al., *Macrophage spatial heterogeneity in gastric cancer defined by multiplex immunohistochemistry.* Nature communications, 2019. **10**(1): p. 3928.

14. Long, W., Y. Yang, and H.-B. Shen, *ImPLoc: a multi-instance deep learning model for the prediction of protein subcellular localization based on immunohistochemistry images.* Bioinformatics, 2020. **36**(7): p. 2244-2250.
15. Rueda, O.M., et al., *Dynamics of breast-cancer relapse reveal late-recurring ER-positive genomic subgroups.* Nature, 2019. **567**(7748): p. 399-404.
16. Asavasupreechar, T., et al., *Systemic distribution of progesterone receptor subtypes in human tissues.* The Journal of steroid biochemistry and molecular biology, 2020. **199**: p. 105599.
17. Liang, Q., et al., *Effect of Ki-67 expression levels and histological grade on breast cancer early relapse in patients with different immunohistochemical-based subtypes.* Scientific reports, 2020. **10**(1): p. 7648.
18. Tsai, Y.F., et al., *HER2 immunohistochemical scores provide prognostic information for patients with HER2-type invasive breast cancer.* Histopathology, 2019. **74**(4): p. 578-586.
19. Magaki, S., et al., *An introduction to the performance of immunohistochemistry.* Biobanking: methods and protocols, 2019: p. 289-298.
20. Van Bockstal, M., et al., *A plea for appraisal and appreciation of immunohistochemistry in the assessment of prognostic and predictive markers in invasive breast cancer.* The Breast, 2018. **37**: p. 52-55.
21. Alexander, S.P., et al., *Goals and practicalities of immunoblotting and immunohistochemistry: A guide for submission to the British Journal of Pharmacology.* British journal of pharmacology, 2018. **175**(3): p. 407.
22. Kashyap, A., et al., *Quantitative microimmunohistochemistry for the grading of immunostains on tumour tissues.* Nature biomedical engineering, 2019. **3**(6): p. 478-490.
23. Noland, E.L. and M. Kiupel, *Coexpression of CD3 and CD20 in canine enteropathy-associated T-cell lymphoma.* Veterinary pathology, 2018. **55**(2): p. 241-244.
24. Lerner, G., et al., *AMACR expression is a potential diagnostic marker in apocrine lesions of breast, and is Associated with high histologic Grade and Lymph Node metastases in some invasive apocrine breast cancers.* Clinical Breast Cancer, 2023. **23**(2): p. 199-210.
25. Harms, P.W., et al., *Multiplex immunohistochemistry and immunofluorescence: a practical update for pathologists.* Modern Pathology, 2023. **36**(7): p. 100197.
26. Laberiano-Fernández, C., et al., *Best practices for technical reproducibility assessment of multiplex immunofluorescence.* Frontiers in Molecular Biosciences, 2021. **8**: p. 660202.

27. Wilson, C.M., et al., *Challenges and opportunities in the statistical analysis of multiplex immunofluorescence data.* Cancers, 2021. **13**(12): p. 3031.
28. Hernandez, S., et al., *Multiplex immunofluorescence tyramide signal amplification for immune cell profiling of paraffin-embedded tumor tissues.* Frontiers in molecular biosciences, 2021. **8**: p. 667067.
29. Ehrenberg, A.J., et al., *A manual multiplex immunofluorescence method for investigating neurodegenerative diseases.* Journal of neuroscience methods, 2020. **339**: p. 108708.
30. Eng, J., et al., *Cyclic multiplexed-immunofluorescence (cmIF), a highly multiplexed method for single-cell analysis.* Biomarkers for Immunotherapy of Cancer: Methods and Protocols, 2020: p. 521-562.
31. Goossens, P., et al., *Integrating multiplex immunofluorescent and mass spectrometry imaging to map myeloid heterogeneity in its metabolic and cellular context.* Cell metabolism, 2022. **34**(8): p. 1214-1225. e6.
32. Lin, J.-R., M. Fallahi-Sichani, and P.K. Sorger, *Highly multiplexed imaging of single cells using a high-throughput cyclic immunofluorescence method.* Nature communications, 2015. **6**(1): p. 8390.
33. Lin, J.-R., et al., *Highly multiplexed immunofluorescence imaging of human tissues and tumors using t-CyCIF and conventional optical microscopes.* elife, 2018. **7**.
34. Sims, Z., G.B. Mills, and Y.H. Chang, *MIM-CyCIF: masked imaging modeling for enhancing cyclic immunofluorescence (CyCIF) with panel reduction and imputation.* Communications Biology, 2024. **7**(1): p. 409.
35. Limbeck, A., et al., *Methodology and applications of elemental mapping by laser induced breakdown spectroscopy.* Analytica chimica acta, 2021. **1147**: p. 72-98.
36. Zhou, M., et al., *Targeted mass spectrometry to quantify brain-derived cerebrospinal fluid biomarkers in Alzheimer's disease.* Clinical proteomics, 2020. **17**: p. 1-14.
37. Todd, A.R., et al., *Higher resolution charge detection mass spectrometry.* Analytical chemistry, 2020. **92**(16): p. 11357-11364.
38. Liu, R., et al., *Metal stable isotope tagging: renaissance of radioimmunoassay for multiplex and absolute quantification of biomolecules.* Accounts of chemical research, 2016. **49**(5): p. 775-783.
39. McAlister, G.C., et al., *Increasing the multiplexing capacity of TMTs using reporter ion isotopologues with isobaric masses.* Analytical chemistry, 2012. **84**(17): p. 7469-7478.
40. Zhong, X., et al., *Mass barcode signal amplification for multiplex allergy diagnosis by MALDI-MS.* Analytical chemistry, 2016. **88**(12): p. 6184-6189.

41. Ahmad, R., et al., *Barcode DNA-mediated signal amplifying strategy for ultrasensitive biomolecular detection on matrix-assisted laser desorption ionization time of flight (MALDI-TOF) mass spectrometry.* Analytical chemistry, 2017. **89**(17): p. 8966-8973.
42. Nakama, T., et al., *Allosteric regulation of DNAzyme activities through intrastrand transformation induced by Cu (II)-mediated artificial base pairing.* Journal of the American Chemical Society, 2020. **142**(22): p. 10153-10162.
43. Oluwole, A.O., et al., *Peptidoglycan biosynthesis is driven by lipid transfer along enzyme-substrate affinity gradients.* Nature Communications, 2022. **13**(1): p. 2278.
44. Pareek, V., et al., *Metabolomics and mass spectrometry imaging reveal channeled de novo purine synthesis in cells.* Science, 2020. **368**(6488): p. 283-290.
45. Brodbelt, J.S., L.J. Morrison, and I. Santos, *Ultraviolet photodissociation mass spectrometry for analysis of biological molecules.* Chemical reviews, 2019. **120**(7): p. 3328-3380.
46. Zhong, X., H. Chen, and R.N. Zare, *Ultrafast enzymatic digestion of proteins by microdroplet mass spectrometry.* Nature communications, 2020. **11**(1): p. 1049.
47. Heumann, K.G., *Isotope dilution mass spectrometry.* International Journal of Mass Spectrometry and Ion Processes, 1992. **118**: p. 575-592.
48. Nicolardi, S., et al., *Structural characterization of biofunctionalized gold nanoparticles by ultrahigh-resolution mass spectrometry.* ACS nano, 2017. **11**(8): p. 8257-8264.
49. Pham, T.A., et al., *A macrocyclic chelator that selectively binds Ln4+ over Ln3+ by a factor of 1029.* Inorganic chemistry, 2016. **55**(20): p. 9989-10002.
50. He, Y., et al., *Combination of magnetic-beads-based multiple metal nanoparticles labeling with hybridization chain reaction amplification for simultaneous detection of multiple cancer cells with inductively coupled plasma mass spectrometry.* Analytical chemistry, 2018. **91**(1): p. 1171-1177.
51. Hu, J., et al., *Mass spectrometric biosensing: A powerful approach for multiplexed analysis of clinical biomolecules.* ACS sensors, 2021. **6**(10): p. 3517-3535.
52. Havugimana, P.C., et al., *Scalable multiplex co-fractionation/mass spectrometry platform for accelerated protein interactome discovery.* Nature communications, 2022. **13**(1): p. 4043.

53. Gualda, E.J., et al., *Three-dimensional imaging flow cytometry through light-sheet fluorescence microscopy.* Cytometry Part A, 2017. **91**(2): p. 144-151.
54. Prussin, C. and D.D. Metcalfe, *Detection of intracytoplasmic cytokine using flow cytometry and directly conjugated anti-cytokine antibodies.* Journal of immunological methods, 1995. **188**(1): p. 117-128.
55. Chiarella, A.M., et al., *Dose-dependent activation of gene expression is achieved using CRISPR and small molecules that recruit endogenous chromatin machinery.* Nature biotechnology, 2020. **38**(1): p. 50-55.
56. Cossarizza, A., et al., *Guidelines for the use of flow cytometry and cell sorting in immunological studies.* European journal of immunology, 2021. **51**(12): p. 2708-3145.
57. Hensel, J.A., et al., *Identification of splice regulators of fibronectin-EIIIA and EIIIB by direct measurement of exon usage in a flow-cytometry based CRISPR screen.* Scientific Reports, 2021. **11**(1): p. 19835.
58. Shin, H., et al., *Quantifying the level of nanoparticle uptake in mammalian cells using flow cytometry.* Nanoscale, 2020. **12**(29): p. 15743-15751.
59. Robinson, J.P., *Flow cytometry: past and future.* Biotechniques, 2022. **72**(4): p. 159-169.
60. Novo, D., G. Grégori, and B. Rajwa, *Generalized unmixing model for multispectral flow cytometry utilizing nonsquare compensation matrices.* Cytometry Part A, 2013. **83**(5): p. 508-520.
61. ul Rehman, A. and S.A. Qureshi, *A review of the medical hyperspectral imaging systems and unmixing algorithms' in biological tissues.* Photodiagnosis and Photodynamic Therapy, 2021. **33**: p. 102165.
62. Ortega, S., et al., *Hyperspectral and multispectral imaging in digital and computational pathology: a systematic review.* Biomedical Optics Express, 2020. **11**(6): p. 3195-3233.
63. Awad, M.M., *Forest mapping: a comparison between hyperspectral and multispectral images and technologies.* Journal of Forestry Research, 2018. **29**(5): p. 1395-1405.
64. Dian, R., et al., *Recent advances and new guidelines on hyperspectral and multispectral image fusion.* Information Fusion, 2021. **69**: p. 40-51.
65. Abramov, P., et al., *Quantum-cascade lasers in medicine and biology.* Journal of Applied Spectroscopy, 2019. **86**: p. 1-26.
66. Shoshanim, O. and A. Baratz, *A new fluorescence-based methodology for studying bioaerosol scavenging processes using a hyperspectral LIF-LIDAR remote sensing system.* Environmental Research, 2023. **217**: p. 114859.

67. Xu, Z., Y. Jiang, and S. He, *Multi-mode microscopic hyperspectral imager for the sensing of biological samples.* Applied Sciences, 2020. **10**(14): p. 4876.
68. Ortega, S., et al. *Hyperspectral imaging and deep learning for the detection of breast cancer cells in digitized histological images*. in *Medical imaging 2020: Digital pathology*. 2020. SPIE.
69. Fei, B., *Hyperspectral imaging in medical applications,* in *Data handling in science and technology*. 2019, Elsevier. p. 523-565.
70. Halicek, M., et al., *In-vivo and ex-vivo tissue analysis through hyperspectral imaging techniques: revealing the invisible features of cancer.* Cancers, 2019. **11**(6): p. 756.
71. Liu, X., et al., *Fast fluorescence lifetime imaging techniques: A review on challenge and development.* Journal of Innovative Optical Health Sciences, 2019. **12**(05): p. 1930003.
72. Lagarto, J.L., et al., *Real-time multispectral fluorescence lifetime imaging using Single Photon Avalanche Diode arrays.* Scientific Reports, 2020. **10**(1): p. 8116.
73. Datta, R., et al., *Fluorescence lifetime imaging microscopy: fundamentals and advances in instrumentation, analysis, and applications.* Journal of biomedical optics, 2020. **25**(7): p. 071203-071203.
74. Sarder, P., D. Maji, and S. Achilefu, *Molecular probes for fluorescence lifetime imaging.* Bioconjugate chemistry, 2015. **26**(6): p. 963-974.
75. Okabe, K., et al., *Intracellular temperature mapping with a fluorescent polymeric thermometer and fluorescence lifetime imaging microscopy.* Nature communications, 2012. **3**(1): p. 705.
76. Totland, C., et al., *A broad-range fluorescence lifetime pH sensing material based on a single organic fluorophore.* Journal of Fluorescence, 2019. **29**: p. 1125-1131.
77. Wu, S., et al., *Polarity-sensitive and membrane-specific probe quantitatively monitoring ferroptosis through fluorescence lifetime imaging.* Analytical Chemistry, 2022. **94**(32): p. 11238-11247.
78. Berezin, M.Y. and S. Achilefu, *Fluorescence lifetime measurements and biological imaging.* Chemical reviews, 2010. **110**(5): p. 2641-2684.
79. Pandey, S. and D. Bodas, *High-quality quantum dots for multiplexed bioimaging: A critical review.* Advances in Colloid and Interface Science, 2020. **278**: p. 102137.
80. Lakowicz, J.R., *Quenching of fluorescence.* Principles of fluorescence spectroscopy, 1983: p. 257-301.
81. Venkatesan, M., et al., *Evolution of electrospun nanofibers fluorescent and colorimetric sensors for environmental toxicants, pH, temperature, and*

*cancer cells–A review with insights on applications.* Chemical Engineering Journal, 2020. **397**: p. 125431.
82. Yang, X., et al., *Recent advances in multifunctional fluorescent probes for viscosity and analytes.* Coordination Chemistry Reviews, 2022. **453**: p. 214336.
83. Xiao, H., P. Li, and B. Tang, *Recent progresses in fluorescent probes for detection of polarity.* Coordination Chemistry Reviews, 2021. **427**: p. 213582.
84. Dangi, V., M. Baral, and B. Kanungo, *Photophysical Studies of a Catechol Based Polyfunctional Dipodal Chelator: Application for Optical Probe for Selective Detection of Fe (III).* Journal of Fluorescence, 2020. **30**: p. 1131-1149.
85. Cravcenco, A., et al., *Interplay between Förster and Dexter Energy Transfer Rates in Isomeric Donor–Bridge–Acceptor Systems.* The Journal of Physical Chemistry A, 2020. **124**(36): p. 7219-7227.
86. Madhu, M., et al., *Directed self-assembly of Ag+-deposited MoS2 quantum dots for colorimetric, fluorescent and fluorescence-lifetime sensing of alkaline phosphatase.* Analytical and Bioanalytical Chemistry, 2022. **414**(5): p. 1909-1919.
87. Jares-Erijman, E.A. and T.M. Jovin, *FRET imaging.* Nature biotechnology, 2003. **21**(11): p. 1387-1395.
88. Karpf, S., et al., *Spectro-temporal encoded multiphoton microscopy and fluorescence lifetime imaging at kilohertz frame-rates.* Nature communications, 2020. **11**(1): p. 2062.
89. Rahim, M.K., et al., *Phasor analysis of fluorescence lifetime enables quantitative multiplexed molecular imaging of three probes.* Analytical chemistry, 2022. **94**(41): p. 14185-14194.
90. Wright, B.K., et al., *NADH distribution in live progenitor stem cells by phasor-fluorescence lifetime image microscopy.* Biophysical journal, 2012. **103**(1): p. L7-L9.
91. Gratton, E., et al., *Fluorescence lifetime imaging for the two-photon microscope: time-domain and frequency-domain methods.* Journal of biomedical optics, 2003. **8**(3): p. 381-390.
92. Elson, D., et al., *Time-domain fluorescence lifetime imaging applied to biological tissue.* Photochemical & Photobiological Sciences, 2004. **3**: p. 795-801.
93. Liang, Z., et al., *Quantifying nuclear wide chromatin compaction by phasor analysis of histone Förster resonance energy transfer (FRET) in frequency domain fluorescence lifetime imaging microscopy (FLIM) data.* Data in Brief, 2020. **30**: p. 105401.

94. Mannam, V., et al., *Machine learning for faster and smarter fluorescence lifetime imaging microscopy.* Journal of Physics: Photonics, 2020. **2**(4): p. 042005.
95. Digman, M.A., et al., *The phasor approach to fluorescence lifetime imaging analysis.* Biophysical journal, 2008. **94**(2): p. L14-L16.
96. Ranjit, S., et al., *Fit-free analysis of fluorescence lifetime imaging data using the phasor approach.* Nature protocols, 2018. **13**(9): p. 1979-2004.
97. Malacrida, L., et al., *The phasor plot: a universal circle to advance fluorescence lifetime analysis and interpretation.* Annual Review of Biophysics, 2021. **50**: p. 575-593.
98. Vallmitjana, A., et al., *Blind resolution of lifetime components in individual pixels of fluorescence lifetime images using the phasor approach.* The journal of physical chemistry B, 2020. **124**(45): p. 10126-10137.
99. Torrado, B., L. Malacrida, and S. Ranjit, *Linear combination properties of the phasor space in fluorescence imaging.* Sensors, 2022. **22**(3): p. 999.
100. Malacrida, L., *Phasor plots and the future of spectral and lifetime imaging.* Nature Methods, 2023. **20**(7): p. 965-967.
101. Modena, M.M., et al., *Nanoparticle characterization: what to measure?* Advanced Materials, 2019. **31**(32): p. 1901556.
102. Griffin, S., et al., *Natural nanoparticles: a particular matter inspired by nature.* Antioxidants, 2017. **7**(1): p. 3.
103. Eivazzadeh-Keihan, R., et al., *Functionalized magnetic nanoparticles for the separation and purification of proteins and peptides.* TrAC Trends in Analytical Chemistry, 2021. **141**: p. 116291.
104. Hong, J., et al., *Foliar application of nanoparticles: mechanisms of absorption, transfer, and multiple impacts.* Environmental Science: Nano, 2021. **8**(5): p. 1196-1210.
105. Gavas, S., S. Quazi, and T.M. Karpiński, *Nanoparticles for cancer therapy: current progress and challenges.* Nanoscale research letters, 2021. **16**(1): p. 173.
106. Georgilis, E., et al., *Nanoparticles based on natural, engineered or synthetic proteins and polypeptides for drug delivery applications.* International journal of pharmaceutics, 2020. **586**: p. 119537.
107. Shi, L., et al., *Effects of polyethylene glycol on the surface of nanoparticles for targeted drug delivery.* Nanoscale, 2021. **13**(24): p. 10748-10764.
108. Salata, O.V., *Applications of nanoparticles in biology and medicine.* Journal of nanobiotechnology, 2004. **2**: p. 1-6.
109. De, M., P.S. Ghosh, and V.M. Rotello, *Applications of nanoparticles in biology.* Advanced Materials, 2008. **20**(22): p. 4225-4241.

110. Curley, S.M. and D. Putnam, *Biological nanoparticles in vaccine development.* Frontiers in Bioengineering and Biotechnology, 2022. **10**: p. 867119.
111. Martín-Moreno, A., et al., *Nanoparticle-delivered HIV peptides to dendritic cells a promising approach to generate a therapeutic vaccine.* Pharmaceutics, 2020. **12**(7): p. 656.
112. Liu, X., et al., *Noble metal–metal oxide nanohybrids with tailored nanostructures for efficient solar energy conversion, photocatalysis and environmental remediation.* Energy & Environmental Science, 2017. **10**(2): p. 402-434.
113. Tong, X., et al., *Enhanced catalytic activity for methanol electro-oxidation of uniformly dispersed nickel oxide nanoparticles—carbon nanotube hybrid materials.* small, 2012. **8**(22): p. 3390-3395.
114. Sankar, M., et al., *Role of the support in gold-containing nanoparticles as heterogeneous catalysts.* Chemical reviews, 2020. **120**(8): p. 3890-3938.
115. Ryoo, R., et al., *Rare-earth–platinum alloy nanoparticles in mesoporous zeolite for catalysis.* Nature, 2020. **585**(7824): p. 221-224.
116. Asadian, E., M. Ghalkhani, and S. Shahrokhian, *Electrochemical sensing based on carbon nanoparticles: A review.* Sensors and Actuators B: Chemical, 2019. **293**: p. 183-209.
117. Croissant, J.G., et al., *Synthetic amorphous silica nanoparticles: toxicity, biomedical and environmental implications.* Nature Reviews Materials, 2020. **5**(12): p. 886-909.
118. Keller, C.B. and T.M. Harrison, *Constraining crustal silica on ancient Earth.* Proceedings of the National Academy of Sciences, 2020. **117**(35): p. 21101-21107.
119. Shortland, A.J. and M.S. Tite, *Raw materials of glass from Amarna and implications for the origins of Egyptian glass.* Archaeometry, 2000. **42**(1): p. 141-151.
120. Jackson, M.D., et al., *Extreme durability in ancient Roman concretes.* Am. Ceram. Soc. Bull, 2018. **97**(5): p. 22-28.
121. Sun, Y., et al., *Change of exposure response over time and long-term risk of silicosis among a cohort of Chinese pottery workers.* International Journal of Environmental Research and Public Health, 2011. **8**(7): p. 2923-2936.
122. Brinker, C.J., K.S. Butler, and S.H. Garofalini, *Are nearly free silanols a unifying structural determinant of silica particle toxicity?* Proceedings of the National Academy of Sciences, 2020. **117**(48): p. 30006-30008.
123. Mehmood, A., et al., *Mesoporous silica nanoparticles: a review.* J. Dev. Drugs, 2017. **6**(02).

124. Jeelani, P.G., et al., *Multifaceted application of silica nanoparticles. A review.* Silicon, 2020. **12**(6): p. 1337-1354.
125. Li, H., et al., *Functionalized silica nanoparticles: classification, synthetic approaches and recent advances in adsorption applications.* Nanoscale, 2021. **13**(38): p. 15998-16016.
126. Jadhav, S.A., et al., *Recent advancements in silica nanoparticles based technologies for removal of dyes from water.* Colloid and Interface Science Communications, 2019. **30**: p. 100181.
127. Niculescu, V.-C., *Mesoporous silica nanoparticles for bio-applications.* Frontiers in Materials, 2020. **7**: p. 36.
128. Baccile, N., D. Grosso, and C. Sanchez, *Aerosol generated mesoporous silica particles.* Journal of Materials Chemistry, 2003. **13**(12): p. 3011-3016.
129. Al-Abboodi, S.M.T., E.J.A. Al-Shaibani, and E.A. Alrubai. *Preparation and characterization of nano silica prepared by different precipitation methods*. in *IOP Conference Series: Materials Science and Engineering*. 2020. IOP Publishing.
130. Masalov, V., et al., *Mechanism of formation and nanostructure of Stöber silica particles.* Nanotechnology, 2011. **22**(27): p. 275718.
131. Ren, D., et al., *Controlled synthesis of mesoporous silica nanoparticles with tunable architectures via oil-water microemulsion assembly process.* Colloids and Surfaces A: Physicochemical and Engineering Aspects, 2021. **611**: p. 125773.
132. Hyde, E.D., et al., *Colloidal silica particle synthesis and future industrial manufacturing pathways: a review.* Industrial & Engineering Chemistry Research, 2016. **55**(33): p. 8891-8913.
133. Li, Z., Y. Zhang, and N. Feng, *Mesoporous silica nanoparticles: synthesis, classification, drug loading, pharmacokinetics, biocompatibility, and application in drug delivery.* Expert opinion on drug delivery, 2019. **16**(3): p. 219-237.
134. Pratiwi, F.W., et al., *The bioimaging applications of mesoporous silica nanoparticles.* The Enzymes, 2018. **43**: p. 123-153.
135. Natarajan, S.K. and S. Selvaraj, *Mesoporous silica nanoparticles: importance of surface modifications and its role in drug delivery.* RSC advances, 2014. **4**(28): p. 14328-14334.
136. Kankala, R.K., et al., *Nanoarchitectured structure and surface biofunctionality of mesoporous silica nanoparticles.* Advanced materials, 2020. **32**(23): p. 1907035.
137. Gou, K., et al., *Carboxyl-functionalized mesoporous silica nanoparticles for the controlled delivery of poorly water-soluble non-steroidal anti-inflammatory drugs.* Acta Biomaterialia, 2021. **134**: p. 576-592.

138. Jiang, Y., et al., *Magnetic mesoporous silica nanoparticles modified by phosphonate functionalized ionic liquid for selective enrichment of phosphopeptides.* RSC advances, 2022. **12**(41): p. 26859-26865.
139. Martínez-Edo, G., et al., *Glycyrrhetinic acid-functionalized mesoporous silica nanoparticles for the co-delivery of DOX/CPT-PEG for targeting HepG2 cells.* Pharmaceutics, 2020. **12**(11): p. 1048.
140. Rumman, G.A., et al., *Adsorption performance of an amine-functionalized MCM–41 mesoporous silica nanoparticle system for ciprofloxacin removal.* Environmental Nanotechnology, Monitoring & Management, 2021. **16**: p. 100536.
141. Yu, Q., et al., *Supramolecular assemblies of heterogeneous mesoporous silica nanoparticles to co-deliver antimicrobial peptides and antibiotics for synergistic eradication of pathogenic biofilms.* Acs Nano, 2020. **14**(5): p. 5926-5937.
142. Wu, X., et al., *pH and thermo dual-stimuli-responsive drug carrier based on mesoporous silica nanoparticles encapsulated in a copolymer–lipid bilayer.* ACS applied materials & interfaces, 2013. **5**(21): p. 10895-10903.
143. Alfhaid, L.H.K., *Recent advance in functionalized mesoporous silica nanoparticles with stimuli-responsive polymer brush for controlled drug delivery.* Soft Materials, 2022. **20**(3): p. 364-378.
144. Chen, F., et al., *Ultrasmall targeted nanoparticles with engineered antibody fragments for imaging detection of HER2-overexpressing breast cancer.* Nature communications, 2018. **9**(1): p. 4141.
145. Madajewski, B., et al., *Molecular engineering of ultrasmall silica nanoparticle–drug conjugates as lung cancer therapeutics.* Clinical Cancer Research, 2020. **26**(20): p. 5424-5437.
146. Wu, F., et al., *Molecular Engineering of Surface Functional Groups Enabling Clinical Translation of Nanoparticle–Drug Conjugates.* Chemistry of Materials, 2022. **34**(12): p. 5344-5355.
147. Zhang, L., et al., *Engineered Ultrasmall Nanoparticle Drug-Immune Conjugates with "Hit and Run" Tumor Delivery to Eradicate Gastric Cancer.* Advanced therapeutics, 2023. **6**(3): p. 2200209.
148. Chen, S., et al., *Biodegradable zinc-containing mesoporous silica nanoparticles for cancer therapy.* Materials Today Advances, 2020. **6**: p. 100066.
149. McCarthy, C.A., et al., *Mesoporous silica formulation strategies for drug dissolution enhancement: a review.* Expert opinion on drug delivery, 2016. **13**(1): p. 93-108.

150. Abdo, G.G., M.M. Zagho, and A. Khalil, *Recent advances in stimuli-responsive drug release and targeting concepts using mesoporous silica nanoparticles.* Emergent Materials, 2020. **3**(3): p. 407-425.
151. Moodley, T. and M. Singh, *Current stimuli-responsive mesoporous silica nanoparticles for cancer therapy.* Pharmaceutics, 2021. **13**(1): p. 71.
152. Al-Kattan, A., et al., *Biological assessment of laser-synthesized silicon nanoparticles effect in two-photon photodynamic therapy on breast cancer MCF-7 cells.* Nanomaterials, 2020. **10**(8): p. 1462.
153. Yuan, D., C.M. Ellis, and J.J. Davis, *Mesoporous silica nanoparticles in bioimaging.* Materials, 2020. **13**(17): p. 3795.
154. Cho, H.-S., et al., *Fluorescent, superparamagnetic nanospheres for drug storage, targeting, and imaging: a multifunctional nanocarrier system for cancer diagnosis and treatment.* ACS nano, 2010. **4**(9): p. 5398-5404.
155. Heidegger, S., et al., *Immune response to functionalized mesoporous silica nanoparticles for targeted drug delivery.* Nanoscale, 2016. **8**(2): p. 938-948.
156. Foda, M.F., et al., *Biocompatible and highly luminescent near-infrared CuInS2/ZnS quantum dots embedded silica beads for cancer cell imaging.* ACS applied materials & interfaces, 2014. **6**(3): p. 2011-2017.
157. Gao, G., et al., *On-off-on fluorescent nanosensor for Fe3+ detection and cancer/normal cell differentiation via silicon-doped carbon quantum dots.* Carbon, 2018. **134**: p. 232-243.
158. Liu, J., et al., *Controlled synthesis of uniform and monodisperse upconversion core/mesoporous silica shell nanocomposites for bimodal imaging.* Chemistry–A European Journal, 2012. **18**(8): p. 2335-2341.
159. Ma, Q., et al., *Multilayered, core/shell nanoprobes based on magnetic ferric oxide particles and quantum dots for multimodality imaging of breast cancer tumors.* Biomaterials, 2012. **33**(33): p. 8486-8494.
160. Chen, F., et al., *In vivo tumor targeting and image-guided drug delivery with antibody-conjugated, radiolabeled mesoporous silica nanoparticles.* ACS nano, 2013. **7**(10): p. 9027-9039.
161. Chen, Y.W., et al., *Mesoporous silica promoted deposition of bioinspired polydopamine onto contrast agent: a universal strategy to achieve both biocompatibility and multiple scale molecular imaging.* Particle & Particle Systems Characterization, 2017. **34**(6): p. 1600415.
162. García de Arquer, F.P., et al., *Semiconductor quantum dots: Technological progress and future challenges.* Science, 2021. **373**(6555): p. eaaz8541.
163. Pohanka, M., *Quantum dots in the therapy: current trends and perspectives.* Mini reviews in medicinal chemistry, 2017. **17**(8): p. 650-656.
164. Yang, Y.-B., et al., *Single virus tracking with quantum dots packaged into enveloped viruses using CRISPR.* Nano Letters, 2020. **20**(2): p. 1417-1427.

165. Zheng, X., et al., *Inkjet-printed quantum dot fluorescent security labels with triple-level optical encryption.* ACS Applied Materials & Interfaces, 2021. **13**(13): p. 15701-15708.
166. Badıllı, U., et al., *Role of quantum dots in pharmaceutical and biomedical analysis, and its application in drug delivery.* TrAC Trends in Analytical Chemistry, 2020. **131**: p. 116013.
167. Sahu, A. and D. Kumar, *Core-shell quantum dots: A review on classification, materials, application, and theoretical modeling.* Journal of Alloys and Compounds, 2022. **924**: p. 166508.
168. Kargozar, S., et al., *Quantum dots: a review from concept to clinic.* Biotechnology Journal, 2020. **15**(12): p. 2000117.
169. Selopal, G.S., et al., *Core/shell quantum dots solar cells.* Advanced Functional Materials, 2020. **30**(13): p. 1908762.
170. Zhang, Y., Y. Li, and X.-P. Yan, *Photoactivated CdTe/CdSe quantum dots as a near infrared fluorescent probe for detecting biothiols in biological fluids.* Analytical chemistry, 2009. **81**(12): p. 5001-5007.
171. Yin, X., et al., *PbS QD-based photodetectors: future-oriented near-infrared detection technology.* Journal of Materials Chemistry C, 2021. **9**(2): p. 417-438.
172. Das, A. and P.T. Snee, *Synthetic developments of nontoxic quantum dots.* ChemPhysChem, 2016. **17**(5): p. 598-617.
173. Chen, B., D. Li, and F. Wang, *InP quantum dots: synthesis and lighting applications.* Small, 2020. **16**(32): p. 2002454.
174. Park, J.-H., et al., *Biodegradable luminescent porous silicon nanoparticles for in vivo applications.* Nature materials, 2009. **8**(4): p. 331-336.
175. Reshma, V., et al., *In vitro and In vivo toxicity analysis of zinc selenium/zinc sulfide (ZnSe/ZnS) quantum dots.* Food and chemical toxicology, 2020. **145**: p. 111718.
176. Rashid, M.H., et al., *Optical dynamics of copper-doped cadmium sulfide (CdS) and zinc sulfide (ZnS) quantum-dots core/shell nanocrystals.* Nanomaterials, 2022. **12**(13): p. 2277.
177. Karimi, F., H.R. Rajabi, and L. Kavoshi, *Rapid sonochemical water-based synthesis of functionalized zinc sulfide quantum dots: study of capping agent effect on photocatalytic activity.* Ultrasonics Sonochemistry, 2019. **57**: p. 139-146.
178. Isac, L. and A. Enesca, *Recent developments in ZnS-based nanostructures photocatalysts for wastewater treatment.* International journal of molecular sciences, 2022. **23**(24): p. 15668.

179. Midya, L., et al., *Novel nanocomposite derived from ZnO/CdS QDs embedded crosslinked chitosan: An efficient photocatalyst and effective antibacterial agent.* Journal of hazardous materials, 2019. **369**: p. 398-407.
180. Liu, M., et al., *Thermodynamic implications of the ligand exchange with alkylamines on the surface of CdSe quantum dots: The importance of ligand–ligand interactions.* The Journal of Physical Chemistry C, 2020. **124**(8): p. 4613-4625.
181. Choi, M.-J., et al., *Ligand exchange at a covalent surface enables balanced stoichiometry in III–V colloidal quantum dots.* Nano letters, 2021. **21**(14): p. 6057-6063.
182. Pham, X.-H., et al., *Synthesis and application of silica-coated quantum dots in biomedicine.* International Journal of Molecular Sciences, 2021. **22**(18): p. 10116.
183. Gao, F., et al., *Highly stable and luminescent silica-coated perovskite quantum dots at nanoscale-particle level via nonpolar solvent synthesis.* Chemical Engineering Journal, 2021. **407**: p. 128001.
184. Shen, J., et al., *A polymer-coated template-confinement CsPbBr 3 perovskite quantum dot composite.* Nanoscale, 2021. **13**(13): p. 6586-6591.
185. Green, M., *The nature of quantum dot capping ligands.* Journal of Materials Chemistry, 2010. **20**(28): p. 5797-5809.
186. Yola, M.L. and N. Atar, *Functionalized graphene quantum dots with bi-metallic nanoparticles composite: sensor application for simultaneous determination of ascorbic acid, dopamine, uric acid and tryptophan.* Journal of The Electrochemical Society, 2016. **163**(14): p. B718.
187. Gao, Y. and X. Peng, *Photogenerated excitons in plain core CdSe nanocrystals with unity radiative decay in single channel: the effects of surface and ligands.* Journal of the American Chemical Society, 2015. **137**(12): p. 4230-4235.
188. Ngouangna, E.N., et al., *Influence of (3–Aminopropyl) triethoxysilane on silica nanoparticle for enhanced oil recovery.* Journal of Molecular Liquids, 2020. **315**: p. 113740.
189. Vasudevan, D., et al., *Core–shell quantum dots: Properties and applications.* Journal of Alloys and Compounds, 2015. **636**: p. 395-404.
190. Björkegren, S.M.S., et al., *Surface activity and flocculation behavior of polyethylene glycol-functionalized silica nanoparticles.* Journal of colloid and interface science, 2015. **452**: p. 215-223.
191. Rahim, M.K., R. Kota, and J.B. Haun, *Enhancing reactivity for bioorthogonal pretargeting by unmasking antibody-conjugated trans-cyclooctenes.* Bioconjugate chemistry, 2015. **26**(2): p. 352-360.